1-1-2017

# Structure-Property Relations of the Exoskeleton of the Ironclad Beetle (Zopherus Nodulosus Haldemani)

Vina Le Nguyen

# Structure-property relations of the exoskeleton of the ironclad beetle (Zopherus nodulosus haldemani)

By

Vina Le Nguyen

A Document Type.
Submitted to the Faculty of
Mississippi State University
in Partial Fulfillment of the Requirements
for the Degree of Master of Science
in Biological Engineering
in the Department of Agricultural and Biological Engineering

Mississippi State, Mississippi

December 2017

Structure-property relations of the exoskeleton of the ironclad beetle (Zopherus nodulosus haldemani)

By

Vina Le Nguyen

Approved:

RajKumar Prabhu
(Major Advisor)

Lakiesha Williams
(Committee Member)

Hongjoo Rhee
(Committee Member)

Mark Horstemeyer
(Committee Member)

Fei Yu
(Graduate Coordinator)

Dean's Name
Dean
Bagley College of Engineering

Name: Vina Le Nguyen

Date of Degree: December 1, 2017

Institution: Mississippi State University

Major Field: Biological Engineering

Major Advisor: Dr. Rajkumar Prabhu

Title of Study: Structure-property relations of the exoskeleton of the ironclad beetle (Zopherus nodulosus haldemani)

Pages in Study: 60

Candidate for Degree of Master of Science

In this study, structure-property relationships in the ironclad beetle (Zopherus nodulosus haldemani) exoskeleton are quantified to develop novel bio-inspired impact resistance technologies. The hierarchical structure of this exoskeleton was observed at various length scales for both the ironclad beetle pronotum and elytron. The exocuticle and endocuticle layers provide the bulk of the structural integrity and consist of chitin-fiber planes arranged in a Bouligand structure. The pronotum consists of a layered structure, while elytron consists of an extra layer with "tunnel-like" voids running along the anteroposterior axis along with smaller interconnecting "tunnel-like" voids in the lateral plane. Energy dispersive X-ray diffraction revealed the existence of minerals such as calcium carbonate, iron oxide, zinc oxide, and manganese oxide. We assert that the strength of this exoskeleton could be attributed to its overall thickness, the epicuticle layer thickness, the existence of various minerals embedded in the exoskeleton, and its structural hierarchy. The thickness of the exoskeleton correlates to a higher number of chitin-fiber planes to increase fracture toughness, while the increased thickness of the epicuticle prevents hydration of the chitin-fiber planes. In previous studies, the existence

of minerals in the exoskeleton has been shown to create a tougher material compared to non-mineralized exoskeletons.

ACKNOWLEDGEMENTS

This effort was sponsored by the Engineer Research and Development Center under Cooperative Agreement number W912HZ-15- 2-0004. The views and conclusions contained herein are those of the authors and should not be interpreted as necessarily representing the official policies or endorsements, either expressed or implied, of the Engineer Research and Development Center or the U.S. Government. In addition, thanks to Mississippi State University's Center for Advanced Vehicular Systems (CAVS), Amanda Lawrence and I-Wei Chu at Institute of Imaging and Analytical Technologies ($I^2$AT), Xanthe Shirley and other students at Texas A&M University's Department of Entomology, and Brett Williams at Engineer Research and Development Center.

TABLE OF CONTENTS

LIST OF TABLES

LIST OF FIGURES

CHAPTER I

INTRODUCTION

## 1.1 Introduction

The following thesis is the first phase of a bio-inspired study on the exoskeleton of the ironclad beetle (*Zopherus nodulosus haldemani*). The text will provide an overview on bio-inspired design and previous studies on arthropod exoskeletons. In addition, the methodology, results, and conclusions of this investigation on the ironclad beetle's exoskeleton structure-property relations will be discussed. Future works will also be provided.

## 1.2 Bio-inspired Design

Bio-inspired design utilizes designs found in nature for man-made material. The study of these structures may provide an optimized design strategy that could be superior to current engineered designs. The study of bio-inspired design allows the analyses of these hierarchical structures. Zolotovsky (2012) defines bio-inspired design as the following three-step process:

1. Study and analyze the system. The identification of main components and their relation to each other.

2. Establish the connection between the components of the system and the functional performance, identification, and quantification of the main parameters in play.

3. Design of new application with similar function performance based on the previous two steps. (Zolotovsky 2012).

Many biomaterials are of interest to bio-inspired design because of their optimal design for a distinct purpose. Biomaterials differ greatly based on the purpose of the material, while biomaterials with a similar purpose may have a similar structure or composition. These differences and underlying similarities in relation to the performance of the system at its purpose provide information that can be used to develop new technology (Liu and Jiang 2011).

Biomaterials that are impact resistance are highly important for bio-inspired design due to their increased ability to improvement future impact resistant technologies. Some of these structures are designed to have higher strength, to have higher stiffness, or to can better absorb energy - the three types of design components that enhances impact resistance (Naleway 2015). These three design components are satisfied along with secondary design requirements such as being lightweight by using different molecular constituents and geometries. Their ability to vary these three variables for impact resistance while satisfying specific secondary needs is non-trivial. The methods of bio-inspired design provide a gateway to the study of natures' systems for future man-made designs.

## 1.3 Arthropod Exoskeletons

### 1.3.1 Hierarchical Structure

All biological structures have a distinct hierarchical structure (Meyers 2008). This means that at different scales (nanoscale, microscale, mesoscale, etc.), there is a structure/feature built upon the structures from the lower length scales. Together, each layer of this hierarchical structure determines the functional and overall efficiency of the system (Lakes 1993).

Arthropod exoskeletons are especially important to these studies because their main purpose is to provide sufficient protection from environmental threats while maintaining the ability to be lightweight while not inhibiting the creature's mobility. The structure of exoskeletons is defined as a fiber-reinforced laminate composite (Chen 2002). However, exoskeletons can vary from hard and brittle to soft and ductile (Jensen and Weis-Fogh 1962) despite having similar structural components. The mechanical properties for exoskeletons vary from species to species and due to the function of the cuticle at a given location on the beetle. This variation is possible due to the varying hierarchical structures. This study focuses on the more impact resistance exoskeletons as found in Crustacea and Insecta sub-phylums.

Exoskeletons are defined as the external skeleton for arthropods. It functions as the protective structure of the organism while offering water impermeability, and muscle attachment (Locke 1964; De Renobales et al. 1991; Noble-Nesbitt 1991). The effectiveness of these functions is dictated by the hierarchical structure. The base "building block" of the hierarchical structure occurs at the molecular scale with N-acetyl-glucosamine molecules (Figure 1.1(a)). As shown in Figure 1.1(b), Chitin is composed of

two linked N-acetyl-glucosamine (Chen 2008). N-acetyl-glucosamine molecules are connected through covalent bonds and form α-chitin chains (Minke 1978). The α-chitin is characterized by the anti-parallel arrangement of chitin chains. The chains are connected through hydrogen bonds to create chitin nanofibrils (Blackwell and Weih 1980). The projection of the N-Acetylglucosamine molecule and the arrangement of the molecules to form α-chitin is shown in Figure 1.1.

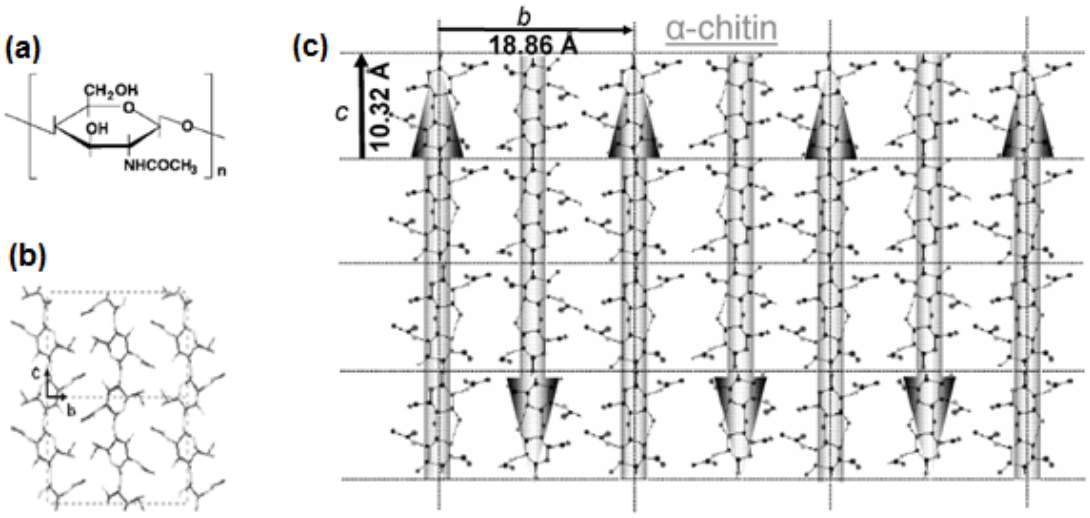


Figure 1.1 (a) Structure of chitin molecule, (b) lattice structure of α-chitin, and (c) structure of chitin nanofibrils (Raabe 2005).

These nanofibrils are surrounded by proteins to form chitin-fibers (Vincent 2004). Figure 1.2 illustrates how the protein surrounds the chitin-fibers. The proteins

surrounding the chitin-fibers have been shown to vary between location in the exoskeleton and by species (Anderson 1995). In most arthropod exoskeletons, the protein is resilin, an elastic structural protein that adds to the bulk of the exoskeleton (Anderson and Weis-Fogh 1964). The chitin-fibers are approximately 300 nm-long and 3-nm thick and are embedded into a protein-mineral plane. Some exoskeletons show evidence of larger nanofibrils where resistance to compression is important. These chitin chains in the nanofibrils are arranged anti-parallel and rely on hydrogen bonding for stiffness and stability (Hillerton and Vincent 1982).

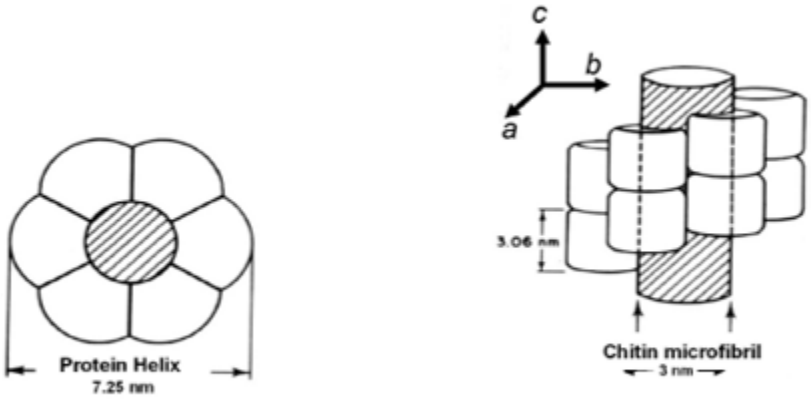


Figure 1.2 Structure of chitin-micro-fibrils (Raabe 2005).

This basic microstructure has been observed in crustacean's exoskeletons and insect's exoskeletons; however, at length scale past the chitin-protein fiber matrix, the cuticle structure begins to diverge based on the subject. At the base, each exoskeleton is a fiber composite consisting of three distinct layers (Hepburn and Chandler 1980). Three

layers are called the epicuticle, exocuticle, and endocuticle from surface to bottom. This is shown in Figure 1.3.

The epicuticle is the dorsal (exterior) layer of the exoskeleton. Its functions are to regulate and control water permeability. It is a composite and consists of three different layers: cuticulin, protein, and waxy layer. The cuticulin layer is the dorsal layer of the epicuticle and is approximately 12 – 13 nm depending on the species. The protein layer is the middle layer of the epicuticle. This layer is penetrated by wax canals connected to pore canals in the procuticle. These wax canals produce the waxy layer of the epicuticle. The waxy layer is on the proximal surface of the exoskeleton. These secrete wax, mixtures of long-chain alcohols, carboxylic acids and hydrocarbons (Wigglesworth 1950). The exact wax composition varies based on the species and diet of the insects (Anderson 1997). This wax layer prevents water permeability of the exoskeleton (Wigglesworth 1972).

The exocuticle and endocuticle are also known as the procuticle and attribute to most of the mechanical properties (Gunderson and Schiavone 1989). An additional layer called the mesocuticle can be found in some insects between the endocuticle and exocuticle (Neville 1984; Andersen 1979; Noble-Nesbitt 1991). These chitin-protein matrices are found in endocuticle and exocuticle. From in-plane scanning electron microscope images, the exoskeleton generally is characterized by pore canals formed by the intersections of parallel chitin-protein matrix. The shape of the canals is purely based on the arrangement of the planes and are not a regular helix (Locke 1961). These pore canals create a honeycomb-like structure on the exoskeletal surface (Sachs 2006). In addition, the pore canals allow more resistance from compressive loading along the

transverse plane. Necking of the pore canals enhances toughness of the structure. Sachs simulated loading and found deformation in the planes were minimized due to the collapse of the pore canals (Sachs 2008; Tong 2004).

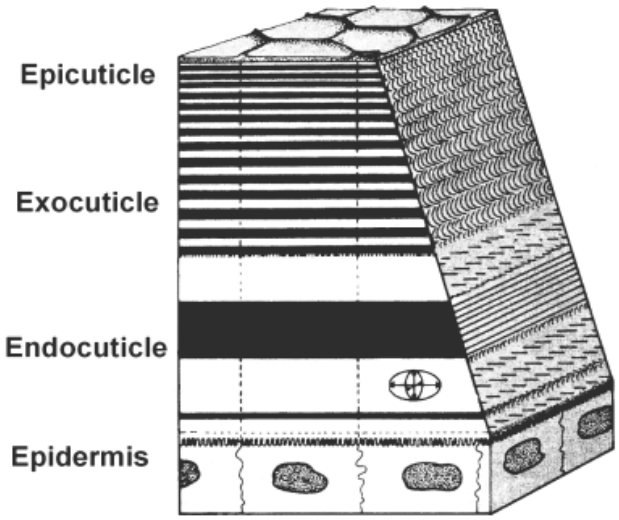


Figure 1.3 The layers of an arthropod exoskeleton (Raabe 2005).

### 1.3.2 Chitin

Chitin is the primary biochemical structure in exoskeletons and, after cellulose, the most abundant natural polysaccharide. It has a theoretically stiffness of 250 GPa, more than twice the stiffness of cellulose, making it the suitable natural material in defensive structures (Vincent 2002). Known for its stiffness, high elastic modulus, and

the primary material in many tough structures, chitin has been studied by many researchers in engineering. According to a study conducted by Chen (2008), chitin is found to be comparable to engineering composites in terms of the function of Young's modulus over density (Chen 2008).

Chitin has been successfully synthesized for numerous uses, increasing the likelihood of developing a bioinspired protective system (Kumar 2000, Fox 2013, Hamed 2016, Wu and Meredith 2014). So, developing a product inspired on a chitin-based structure makes the prototyping of a bioinspired structure is not as difficult a task as other materials.

### 1.3.3 Mineralization

In addition to chitin, the exoskeleton can be hardened by additions of mineral elements such as calcium, zinc, iron, and manganese (Quicke 1998; Hillerton 1984; Al-Sawalmih 2008). In various exoskeletons, minerals can be seen deposited on the nanoscale structure (Lian and Wang 2014; Nikolov 2010; Dittman 2010). The effects of the biomineralization within the exoskeletons have been extensively studied. Iron oxide and manganese oxide have been seen to strengthen soft tissues (Mann 1995; Chen 2008). These minerals, particularly calcium carbonate, have been observed in the microstructure of the exoskeleton at branches of chitin-protein fibers (Fabritius 2009; Locke 1961). In general, the mineral composition of the exocuticle and endocuticle are similar, and thus the higher mechanical properties of the exocuticle cannot be attributed solely by the mineral composition (Fabritius 2009).

## 1.4 Bio-inspired Design Studies Involving Arthropod Exoskeletons

### 1.4.1 Introduction

Impact resistance biomaterials are valuable for bioinspired design. Man-made materials are currently efficient for impact resistance, but not optimal. By analyzing these biomaterials, an optimal design strategy can be discovered. Many biomaterials have been studied thus far such as turtle shells, ram horns, and elk antlers. These materials have a functional purpose of protecting the organism from environmental threats. These materials are made to be permanent and built for a lifetime of damage accumulation.

The design of these permanent biomaterial is different from the design of exoskeletons which are temporary and are not created for damage accumulation. In addition, much of the body is covered in the exoskeletons, and they must be light in weight to not prevent movement of the organism.

All exoskeletons have the same functional properties (lightweight, high strength, mechanical rigidity, and durability), but these properties differentiate depending on type of arthropod, the species, and even the location of the exoskeleton on the body. To further understand this differentiation process, studies have been completed on various crustacean exoskeletons and few insect exoskeletons and are discussed below. These studies also provide a fundamental process that can be applied to the current study.

### 1.4.2 Crustacean Exoskeletons

Crustaceans have been extensively studied due to their ease of sample obtainment. The following studies have analyzed crab and lobster exoskeletons.

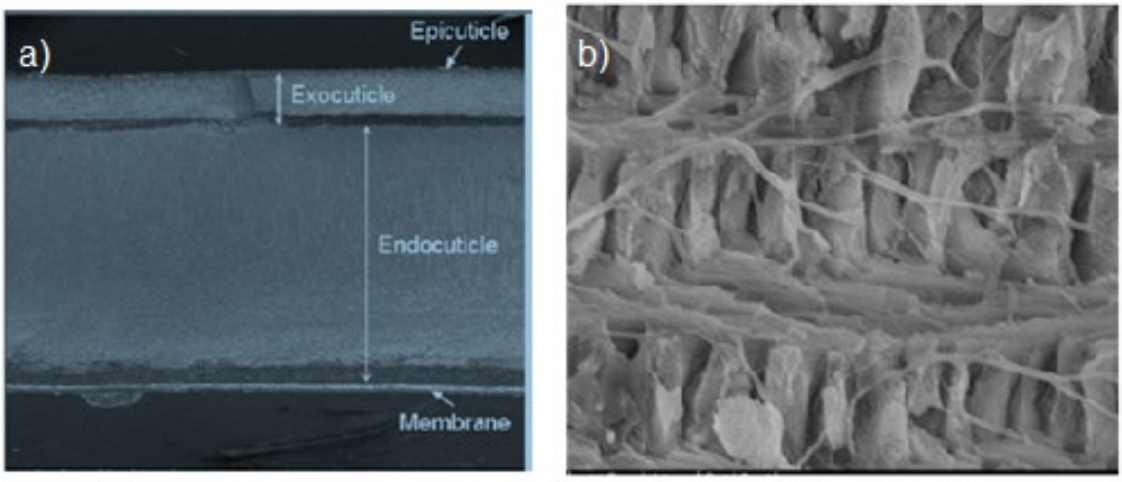


Figure 1.4 SEM images of a) distinct arthropod layers and b) Bouligand structure found in the endocuticle of the Crab Cancer Magister exoskeleton (Lian and Wang 2014).

Crustacean exoskeletons are multilayered composites. Figure 1.4 includes scanning electron microscope (SEM) images showing the layers of the Crab Cancer Magister's exoskeleton. A fourth layer was noted and called the membranous layer. The thickness of each layer depends on the specimen, but typically the epicuticle is the thinnest followed by the exocuticle and endocuticle. The endocuticle and exocuticle were determined to be the primary source of strength within the exoskeleton. Both layers were shown to have a "Bouligand" structure (Lian and Wang 2014). "Bouligand" structure is characterized by a helicoidally stacking sequence of fibrous chitin-protein planes, deposited with calcium carbonate minerals. In addition, the exocuticle was found to have a porous structure, characterized by pore canals within the layered plane (Lian and Wang

2014; Chen 2008). These pore canals allow transport of nutrients through the exoskeleton for formation of new exoskeleton after molting. In addition, it was observed that these pore canals increase the toughness of the structure (Chen 2008).

Using energy dispersive x-rays spectroscopy (EDS or EDX), calcium was found to be the major mineral component of each layer and at an equal percentage in the endocuticle as the exocuticle. The volume of chitin-protein fibers can also be an indicator of high strength in biological composites. Chitin was found in the Crab Cancer Magister's exoskeleton in higher volume in the exocuticle than the endocuticle. From the results of microstructure examination, it is inferred the exocuticle is stronger than the endocuticle because calcium levels were equal, but the exocuticle had a higher volume of chitin. Mechanical testing was completed to determine the strength of the endocuticle and exocuticle, the variation in strength of different locations, and the effect of hydration on the exoskeleton. The mechanical properties were found to decrease with increasing distance into the body (Chen 2008). The hardness values in the exocuticle were almost twice as hard as the endocuticle. Comparing the claw of the Crab Cancer Magister to the body, the claw had almost double the elastic modulus and hardness values as the body shell which is consistent with the function of both structures (Chen 2008; Lian and Wang 2014).

When analyzing the properties of different anatomical features of arthropods and analyzing properties of different species, mechanical properties have been found to different based on the purpose of the structure (Tong 2004, Fabritius 2011). For example, to escape from predators, lobsters typically swim away while crabs typically burrow and live in the sand. Lobsters are optimized with a lighter and more streamline design

(Bosselmann 2007). The crab contained a more mineralized carapace, with 71.6% of the carapace being composed of minerals, while lobsters had a less mineralized carapace with 50% of the carapace being composed of minerals (Bosselmann 2007). This translates into the crab having a highly mineralized, strong carapace while the lobsters had a less mineralized, more elastic carapace. The difference between strength of the lobster and the crab exoskeletons could be related to their flight responses (Bosselmann 2007).

In the lobster exoskeleton, minerals (calcium carbonate) can be seen deposited on the nanoscale structure (Raabe 2006). A figure of mineralization found in the Homarus americanus lobster is shown in Figure 1.5. The minerals can either be amorphous or crystalline calcium carbonate with the addition of magnesium and/or phosphorus (Sachs 2008). The distribution of the mineralization can be seen when the cuticle undergoes deproteination (Romano 2007). The amorphous calcium carbonate is exclusive to the endocuticle, while crystalline calcite is exclusive to the exocuticle (Al-Sawalmih 2008). These minerals were not seen in some exoskeletons such as the Horseshoe crab (Raabe 2005).

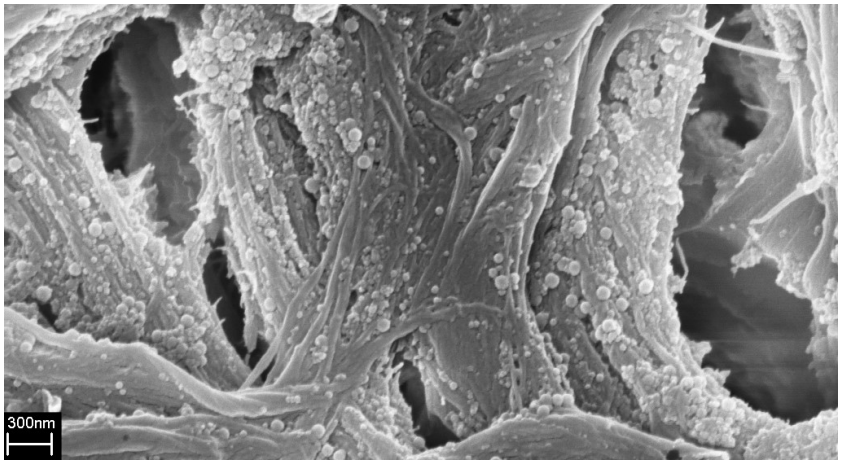


Figure 1.5 Scanning electron microscope images of nanosized particle mineralization found in the Homarus americanus lobster cuticle (Raabe 2005).

The effects of the mineralization on the mechanical properties of the exoskeletons have been extensively studied. The minerals, particularly calcium carbonate, are found in the microstructure at the branches of the exoskeleton (Chen 2008). The initial theories stated that mineral attributes greatly to the overall moduli of the system. In multiscale simulations completed by Nikolov (2011), the amount of minerals in the composition has very little effect on the structure. However, a change in Young's modulus of the minerals contributed for 100% of the difference in the properties (Nikolov 2011). Besides the structural effect of the mineralization, the other effects of minerals have not been determined.

Figure 1.6 shows the hierarchical structure of the *Homarus americanus* lobster. This hierarchical structure is similar to the hierarchical structure of other crustaceans.

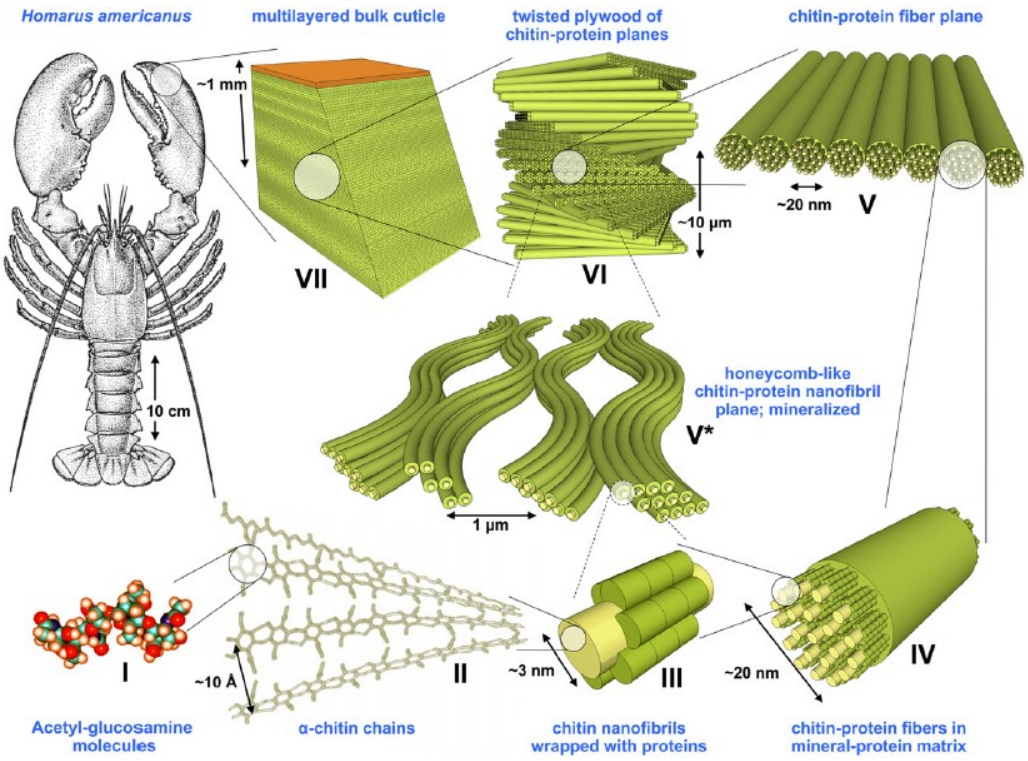


Figure 1.6 The hierarchical structure of the lobster cuticle (Nikolov, 2011).

### 1.4.3 Beetle Exoskeletons

Many studies have characterized the structure and composition of beetle exoskeletons for several species (Hepburn 1973, Sun 2012). Some beetle exoskeletons are like the typical arthropod exoskeleton structure and consists of the basic three layers (epicuticle, exocuticle, and endocuticle). Exocuticle and endocuticle seem relatively the same, both containing variation of chitin-fiber plane volume and being constructed from the Bouligand structure. The epicuticle continues to help keep the exoskeleton

hydrophobic, but in beetles, the epicuticle can contain a certain structural pattern, have specific coloration, or anti-adhesion abilities. The epicuticle surface typically contains a surface with preformed holes (Sun 2012).

Besides the epicuticle, other beetle structures seem to contain a void structure in addition to the basic three layers. For instance, these voids have been seen in the forewing of *Allomyrina dichtoma* beetles and the elytron of various beetles (Chen 2007, Cheng 2002). A diagram of the void structure in the forewing *Allomyrina dichtoma* beetles is shown in Figure 1.7.

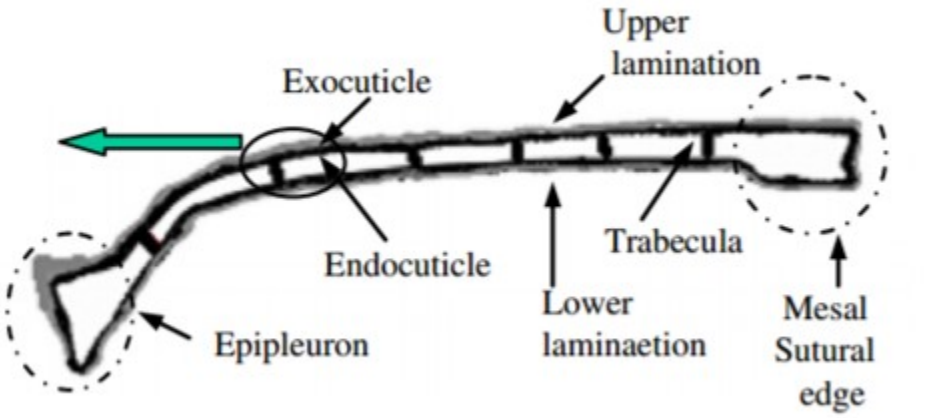


Figure 1.7 Diagram of "void" structure in beetle forewing. Below the endocuticle layer, a series of voids, or air pockets, exist between the "upper" and "lower lamination". The green arrow indicates the direction to rest of insect body (Chen 2007).

The voids are surrounded by continuous chitin-fiber planes. Between each void are trabeculae. Trabeculae contain vertical chitin-fibers and proteins and assist in supporting the structure (Chen 2015). It is believed that the chitin-fibers around the void improve the strength and tolerance of the composite (Gunderson and Lute 1993). The voids are believed to an adaptation of the insect's need for a lightweight exoskeleton, and the trabeculae and continuous chitin-fibers are meant to strengthen the voids.

A study by Sun (2010) analyzed the pull-out of the chitin fibers during micro-tensile testing of the *Copris ochus Mostschulsky* beetle. The study showed that during facture, the chitin-fibers separate from the substrate and then break (Sun 2010). Hepburn and Ball (1973) noted this fracture mechanism is similar to the fracture mechanism in plywood. Plywood, like the Bouligand structure, consists of layers of fibers with each layer being rotated by a certain degree. In both situations, this causes a difficult composite to bend.

Insect exoskeletons have unique design strategies such as the "void" structure allowing strength and lightweight and its Bouligand structure that increases fracture toughness. Further investigation into the design of insect exoskeletons could benefit bio-inspired design.

## 1.5 Ironclad Beetle

### 1.5.1 Introduction

Ironclad beetles can be defined as any species from the subfamily Zopherinae (Foley 2008). Although not much is known about the ironclad beetle in its own habitat, entomologist who attempt to collect the beetle cannot pin the beetle through the exoskeleton. They have to use the force of a drill or a hammer, if the pinning nail or pin is heated to extremely high temperatures (Burke 1976). This led to the assertion that ironclad beetles have one of the most impact resistant exoskeletons of the arthropods. Although common, ironclad beetles are one of the least studied arthropods in any field of science including entomology.

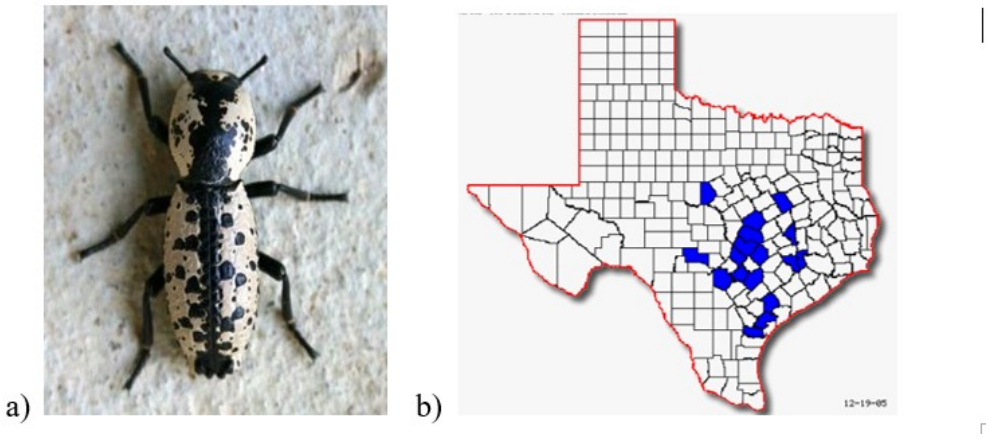


Figure 1.8 a) Ironclad beetle *Zopherus nodulus haldemani* (Barlettt 2014) and b) its known location (Quinn 2017).

This species of ironclad beetle, and others, are found in typically very dry climates such as Southeast Texas. Understanding its acclimation to the dry hotter climate could allow further understanding of its overall structure.

### 1.5.2 Anatomy of Ironclad Beetle

The *Zopherus nodulosus haldemani* is known for its distinct black-and-white pattern on its exoskeleton. This pattern had no defensive significances, but it may affect the chemical composition collected.

Figure 1.9 shows an image of the Ironclad beetle *Zopherus nodulosus haldemani* and the known locations of the ironclad beetle. The main exoskeleton of the ironclad beetle consists of two main parts: pronotum and elytron. The pronotum covers the thorax, while the elytron covers the abdomen. In the figure, the elytron is divided into two parts, elytra, separated by the elytral suture. In flying beetles, the elytra suture would not exist allowing the two elytra to separate and allow forewings to release.

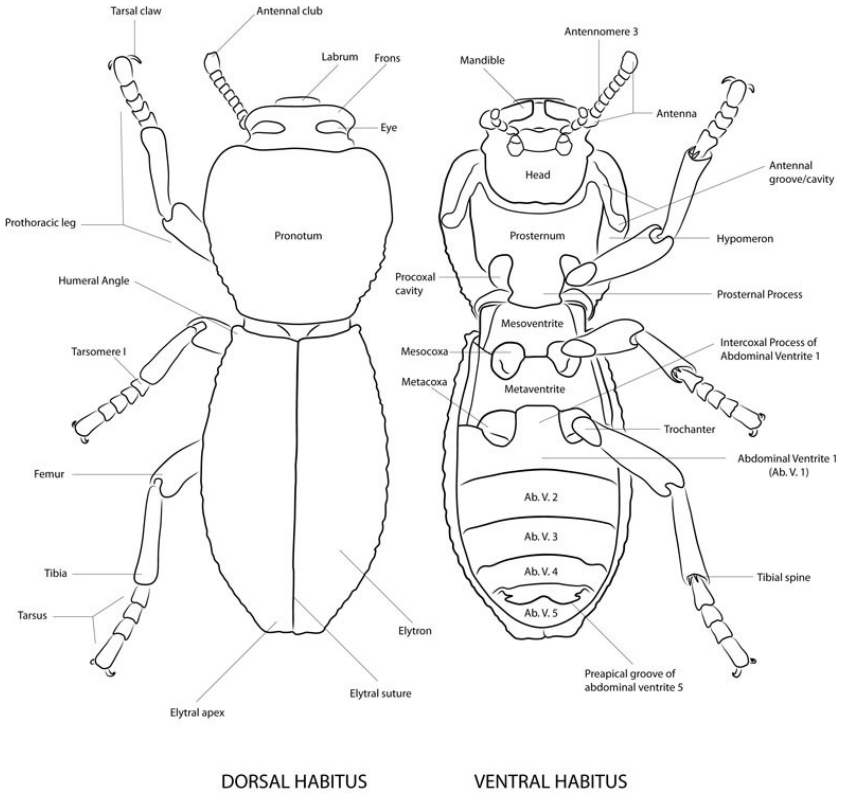


Figure 1.9 Morphological atlas of ironclad beetles (Lord, N.P., Ironclad ID).

This study will focus on analyzing the structure and mechanical properties of the pronotum and elytron.

## 1.6 Study Objectives

The structure and mechanical properties of the ironclad beetle's exoskeleton is unknown. As potentially one of nature's best structures for protection for impact resistance, the ironclad beetle's exoskeleton may provide necessary design strategy for future impact resistant materials.

As outlined by bio-inspired design methods, the study will quantify the structure-property relationship of the ironclad beetle's exoskeleton to identify key components of the system and study their relations to one another. The following goals of the thesis thus follows:

1. Verify the importance of the exoskeleton as a critical subject for bio-inspired design.
2. Study the hierarchical design of the exoskeleton.
3. Determine the mechanical properties of the exoskeleton through nanoindentation.
4. Create relations between the microstructure and mechanical properties for a better understanding of the material.

These studies provide a framework for future bioinspired design strategies inspired insects with hard outer shells (exoskeletons). This study will begin with a microstructure and structure-property components. The microstructure will be observed using SEM and an optical microscope, while the structure-property component will be examined through nanoindentation.

The structure-property relations observed in this study will provide a foundation for the development of an Internal State Variable (ISV) material model and Finite Element (FE) analysis for future studies. The eventual goal of this bioinspired study is to create a 3-Dimensional (3D) prototype for an impact resistant technology.

CHAPTER II

MICROSTRUCTURE OBSERVATION

## 2.1 Sample Preparation

### 2.1.1 Obtainment

Samples were taken from the exoskeleton of the ironclad beetle species *Zopherus nodulous Haldeman*i. The three beetles were collected in southeastern Texas, and all were approximately 3 cm in length, approximately 1 cm in width at the widest point, and 0.5 cm at the thinnest point. One of the collected ironclad beetles is shown in Figure 2.1.

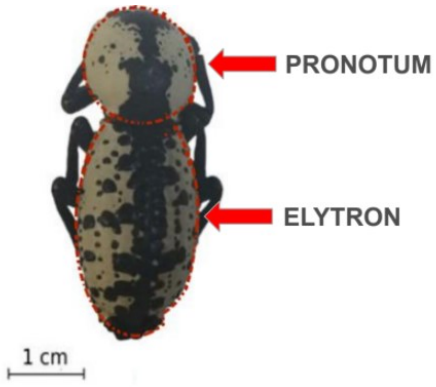


Figure 2.1 Ironclad beetle. Red arrows points to the pronotum and elytron region of the exoskeleton.

The beetle was obtained through donations from collectors related to the Texas A&M University's Department of Entomology. Due to the difficulty of euthanizing the beetles with chemicals and the possibility of effecting the material's structural and mechanical properties through use of chemicals, the beetles were euthanized by freezing per American Veterinary Medicine Association guidelines (Leary 2013).

### 2.1.2 Preparation

In preparation, the specimen was broken through two techniques: fracturing technique using a compression machine and cutting using a diamond saw. A half of the elytra of one beetle was compressed using Instron compression machine EM Model 5869 with a load cell of 50kN to obtain a fractured surface image. The diamond saw was used to achieve cut surface samples, which were then polished following sawing.

## 2.2 Microtomography

MicroCT is a small-scale form of computed tomography (CT). Using x-rays, images slices of a subject is taken and used to generate a 3D model. The Bruker MicroCT (Billerica, MA, USA) was used for structural examination with a resolution of 14.3 µm slice thickness. Using Bruker Skyscan Control (Billerica, MA, USA), 3D reconstruction of the beetle was obtained allowing for analysis of its overall structure.

## 2.3 Scanning Electron Microscopy and the Electron Diffraction X-Ray Spectroscopy

The ironclad beetle samples were mounted to holders using carbon tape and sputter-coated with platinum and observed under a Carl Zeiss EVO50 scanning electron

microscope (Oberkochen, Germany). Samples were coated for 20 seconds and left in machine for 10 minutes after sputter-coating.

### 2.4 Image Analysis

Image analysis was used to analyze MicroCT and SEM images. ImageJ software (National Institutes of Health, Bethesda, MD, USA) and atomic force microscopy (AFM) was used for this process. Various dimensional properties of the exoskeleton such as length and thickness were determined through physical measurements, then incorporated into ImageJ to quantify features such as the thickness of the exoskeleton in various layers and the size of voids found in the cross section of the exoskeleton. AFM with ScanAsyst (Billerica, MA, USA) was used to reveal additional information on the structure of various locations such as length and depth of the surface pattern on the exoskeleton.

The dimensional properties allowed us to compare our ironclad beetle exoskeleton to other exoskeletons and determine possible reasons behind mechanical property differences.

# CHAPTER III

# MECHANICAL TESTING

## 3.1 Nano-indentation

### 3.1.1 Introduction

Nano-indentation was used to measure the hardness (H) and reduced elastic modulus of the material ($E_R$). The hardness of the material correlates to the resistance of compressive deformation, and the elastic modulus describes the material's tendency to deform.

The theories and calculations have been well-established but particularly of Oliver and Pharr (1992).

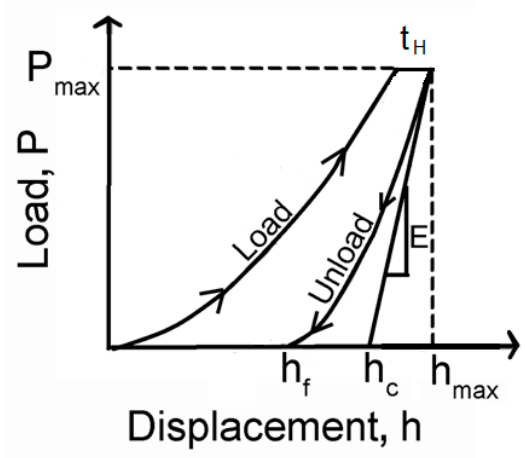


Figure 3.1 Load-unload curve obtained from nanoindentation where E is elastic modulus, $t_H$ is holding time, $h_c$ is contact depth, $h_f$ is final depth, and $h_{max}$ is maximum depth.

The stiffness (S) is experimentally measured as ratio of the change in load (P) and change in displacement (h) (Eq. (1)). Stiffness is used to calculate the reduced elastic modulus, $E_r$ (Eq. (2)).

$$S = \frac{dP}{dh} = \frac{2}{\pi} E_r \sqrt{A} \qquad \text{Eq.(1)}$$

$$Er = \frac{S * pi}{2\sqrt{A}} \qquad \text{Eq.(2)}$$

$$H = \frac{P_{max}}{A} \qquad \text{Eq.(3)}$$

Hardness is calculated using Eq. (3) where H represents the hardness, $P_{max}$ represents the peak load, and A represents the area of the indentation (Oliver and Pharr 1992).

This study utilizes Hysitron Triboindenter (Minneapolis, MS, USA) to complete nano-indentation. All testing utilized a diamond Berkovich tip. The testing is completed by pressing the tip of the indenter to the sample at a known load for a known time. As the tip indents the sample, the tip measures the depth and displacement of the tip and determines the area of the indentation. The size correlates to the fracture properties and its viscous and plastic components (Hillerton 1982).

### 3.1.2 Surface Indentation

The samples were first prepared cutting the exoskeleton using a diamond saw, then polished. Polishing the sample creates a smooth surface to prevent the tip from slipping or providing an inaccurate measurement. The samples were then attached to a surface using hot glue. To avoid the influence of the substrate materials on the measurements of the mechanical properties of the specimen, the penetration depth should be less than 10 percent of the specimen thickness (Fischer-Cripps A.C, Introduction to Contact Mechanics).

Nano-indentation is highly affected by the loading rate, holding time, and indention height. This has shown to be true for arthropod cuticles. A study by Tong (2004) showed the length of loading rate and holding time affected the hardness and elastic modulus calculated. To determine the nano-indentation parameters used in this study, previous nano-indentation parameters were found and altered to suit our material. Nano-indentation parameters used in previous beetle exoskeleton studies are shown in

Table 3.1. In this study, we completed nano-indentation on various locations of the exoskeleton with loading rates of 1, 10, and 100 μN/s. The peak load for the experiment is 1500 μN with a holding time of 20 seconds. The variation of loading rates allows analysis of the mechanical differences in depth and addition analysis of how the material deforms under increased loading rates.

Table 3.1 Nano-indentation parameters from previous studies (Sun 2014, Sun 2007, and Sun 2008)

| **Biomaterial** | **Peak Load (μN)** | **Loading Rate (μN/s)** | **Holding Time (s)** |
|---|---|---|---|
| Elytra Cuticle from a Dung Beetle | 1500 | 53 | 20 |
| Elytra Cuticle from a Dung Beetle | 500 | 53 | 20 |
| Cuticle of *Copris ochus Motschulsky*, | 500 | 53 | 20 |
| Cuticle of *Geotrupes stercorarius Linnaeus* | 500 | 53 | 20 |
| Cuticle of *Holotrichia sichotana Brenske* | 500 | 53 | 20 |

Nano-indentation parameters for various studies on different beetle exoskeletons.

### 3.2 Cross Section Indentation

Due to the layered structure of the pronotum and elytron, nano-indentation was completed along the cross section from the top surface to the bottom surface. This was completed to determine the mechanical properties of each layer and the associated effect on the overall material. Testing was completed with a loading and unloading rate of 10 μN/s, a holding time of 20s, and a peak load of 500 μN. Each sample was cold mounted into epoxy and then polished. In addition to reduced elastic modulus and hardness values, the change in reduced elastic modulus and hardness values with regards to the distance from the top surface was also calculated.

# CHAPTER IV

# RESULTS AND DISCUSSION

## 4.1 Beetle Length Characterization

The ironclad beetles obtained for this study were approximately 2 cm in length. A 3D reconstruction from the microCT scans of the ironclad beetle can be seen in Figure 4.1 in addition to the cross section (transverse plane) of the pronotum and elytron. The thickness calculated from those microCT revealed that the exoskeleton of the ironclad beetle was thicker, with a thickness of pronotum was 0.024 – 0.100 mm and thickness of elytron was 0.275 – 0.510 mm, compared to the exoskeleton of the dung beetle (thickness of 0.6 μm) studied by Tong (2004) and comparable to the crab magister (thickness of 0.8 mm) studied by Lian (2011). The fact that the wings of ironclad beetles are fused into the elytron unlike some types of beetles could attribute to the increased thickness of the elytron in comparison to the pronotum and other beetle exoskeletons (Foley 2006).

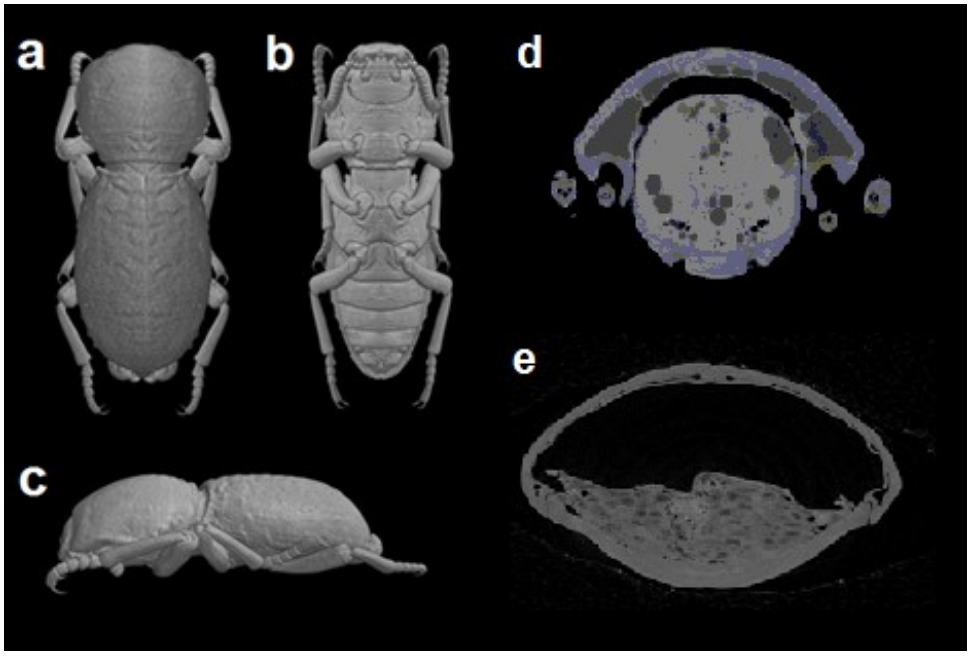


Figure 4.1 Micro CT images of the ironclad beetle were reconstructed in 3D model using Bruker Skyscan Control. The 3D reconstruction is shown from the (a) dorsal view, (b) ventral view, and (c) left side view. MicroCT images show the cross section of the (d) pronotum and (e) elytron (not to scale for visibility).

## 4.2 Surface Analysis of Pronotum and Elytron

The dorsal view of the pronotum and elytron's exoskeleton surfaces is shown in Figure 4.2. These surfaces, which have black and white patterns, were analyzed via SEM and EDS. No structural or chemical differences were found between the black and white sections of the exoskeleton. Both the pronotum and elytron surfaces contain noticeable "scratch-like" lines that lack any pattern or did not contribute functionally to the exoskeleton. It can be asserted that these scratches were caused by environmental damage prior to collection. White spherical objects determined to be either tubercles or debris

from the environment were also located along the surface. Tubercle describes a small rounded projection found on the surface of plants and animals (Merriam-Webster, 2017). The tubercles observed on the surface of the exoskeleton are wax mounds produced by the epicuticle surface. Accumulated environmental debris have been seen by entomologists while analyzing specimens from the Zopherini tribe (Foley 2008). The surface pattern or the wax layer could both be causes of debris accumulation.

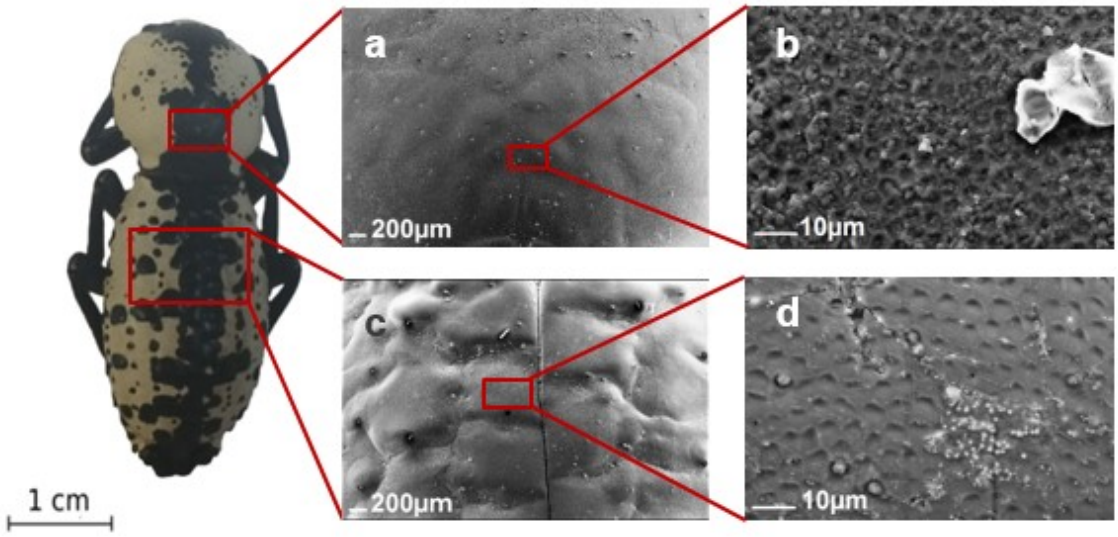


Figure 4.2 SEM images of the surface of the exoskeleton (a), (b) on the pronotum and (c), (d) on the elytron. (a) Surface of the pronotum shows roughness and some pores. (b) Higher magnification of the pronotum surface shows that there are repressions. (c) Surface of the elytron shows hexagonal cells with approximately 400 µm diameter. (d) The higher magnified image on the elytron also reveals that there are depressions with approximately 2-3 µm side length.

At the lower scale, a honeycomb pattern with depressions exists on both the pronotum and elytron. Each side of the honeycomb has side lengths varying between 2 - 3 μm. Figure 4.3 shows the depth of the pattern in addition to images describing the mechanism creating the pattern can be seen. Figure 4.3a shows the pattern that covers majority of the top surface. Figure 4.3b shows the AFM the depth of each pore. Each pore has approximately the same depth of 1.0 μm.

Figure 4.3c shows the cross section of the pronotum and elytron specifically thick epicuticle layer, consisting of wax pore canals, leading from the exoskeleton surface to the exocuticle. They are about 25 μm in thickness. According to Locke, the patterns on the exoskeleton are formed by the deposition of wax by cells of the wax pore canals, a mechanism shown in Figure 4.3d (Locke 1960). The wax is deposited on the edge of the cells causing the observable depression. Locke observed the same pore canal pattern in Calpodes ethlius (Locke 1960). In the cross section of the pronotum and elytron, wax pore canals leading from the exoskeleton surface to the endocuticle was observed. They are about 25 μm in length. These wax pore canals are reported to contain and transfer wax materials to the epicuticle surface to the endocuticle (Wigglesworth 1985). The height of the wax pore canals could be telling of the distance water would have to travel to reach the chitinous regions. In addition to the hydrophobic wax layer, if water was to penetrate, the wax pore canals could prevent it from reaching other inner layers, which will be further discussed in section 4.6.

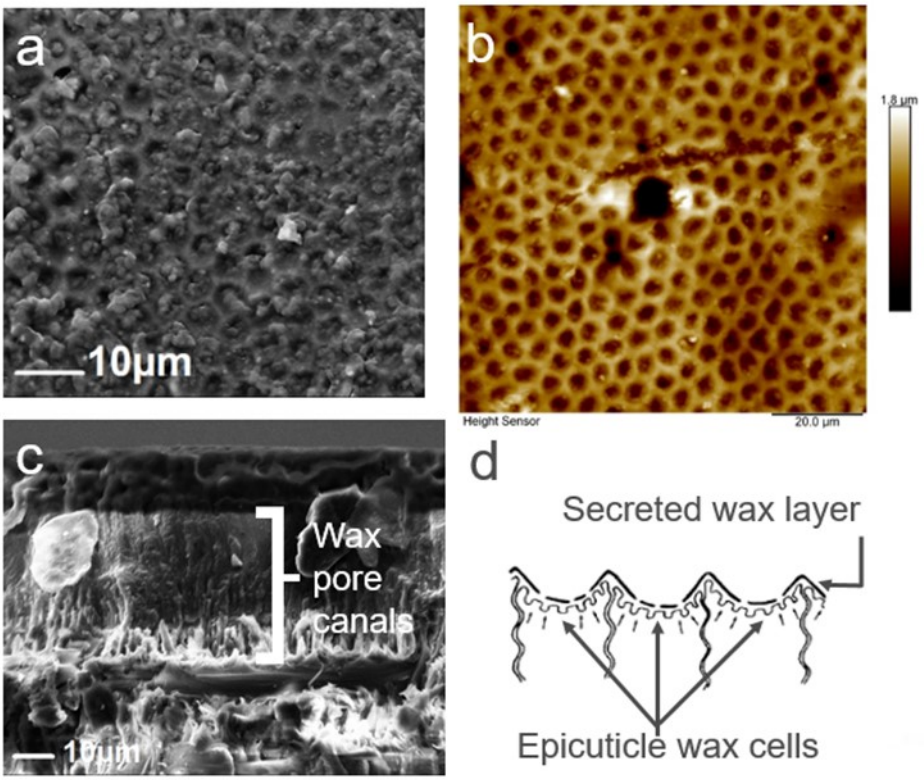


Figure 4.3 (a) SEM image of elytron surface showing honeycomb pattern, (b) AFM image of surface showing height difference of depressions, (c) SEM image of pore wax canals in the epicuticle layer, and (d) a schematic of wax secreting mechanism that results in honeycomb pattern (Foley 2008). Each pore depression has a depth of 1.0 µm.

At a higher scale, a polygonal pattern is seen on the surface of the elytron. This pattern is not seen on the pronotum and is observed to correlate the laminar brick structure of the elytron. Further analysis of this structure is in section 4.4.

## 4.3 Analysis of Cross Section of Exoskeleton

The SEM images on the cross section of the pronotum and elytron is shown in Figure 4.4. Figure 4.4a and 4.4b are the cutting and fracture surfaces of the cross section of the pronotum, and Figure 4.4c and 4.4d are the cutting and fracture surfaces of cross section of the elytron. The cross section images in Figure 4.4 reveals three layers consisting of exoskeleton: pore canals, exocuticle, and endocuticle. In addition, the elytron cross section shows the laminar brick structure consisting of "tunnel-like" voids with chitin-fiber planes surrounding the voids.

Exocuticle and endocuticle have a structure comprising of chitin-fiber planes with the classic Bouligand structure. The Bouligand, or 'twisted plywood', structure is described as a stacking of angled planes that consist of a series of chitin microtubules (Yang 2017). This Bouligand structure has been found in other biological defensive systems, such as other arthropod exoskeletons and *Arapaima gigas* fish scales. Zimmermann states the Bouligand-type structure allows the exoskeleton to reorient in response to loading, increasing the toughness to the material (Zimmerman 2013). The chitin planes arranged in a Bouligand structure are characteristic to arthropod exoskeletons and in the ironclad beetle. The chitin fibers consisting Bouligand structure were measured and found to be approximately 5 μm in diameter. The fractured surface of the pronotum and elytron show the chitin-fibers sections that were pulled out during fracture. The pulling of the chitin fibers removes load and increases the apparent toughness of the structure (Hepburn 1973).

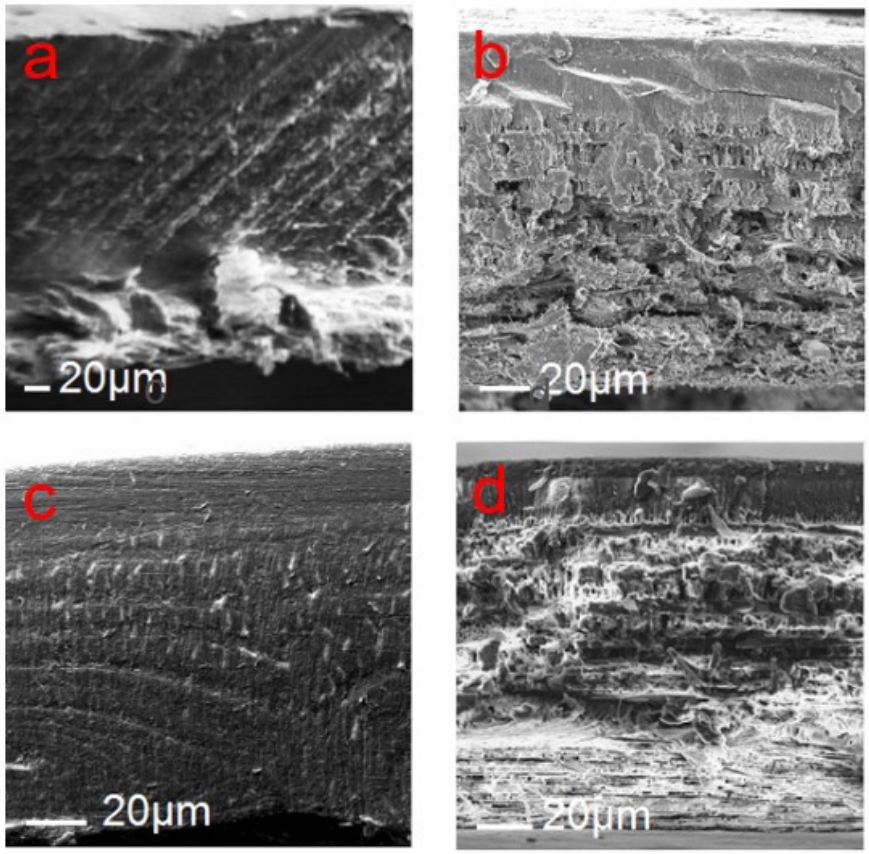


Figure 4.4 Comparison of the (a) cutting surface and (b) fracture surface of the pronotum and (c) cutting surface of elytra and (d) facture surface of elytron.

Furthermore, Chen (2008) reported that while both the claws and shell of the crab Cancer Magister had the same overall thickness, the thickness of the exocuticle and endocuticle varied. This could be a factor in what causes the difference in mechanical properties between these structures (Lian 2014). The endocuticle is known to be less dense in comparison to the exocuticle (Chen 2008). This produces a softer and more flexible material. Due to the decrease in number of chitin-fiber planes with increased

endocuticle thickness, the material could lose strength because there are less chitin-fibers to pull-out during fracture. In the crab magister, the claw had a thicker layer of exocuticle and had the higher mechanical properties possibly indicating a correlation. As in the crab magister, this phenomenon is true in many different insect exoskeletons and could be the cause of the difference in the mechanical properties between the pronotum and elytron in the ironclad beetle (Chen 2008).

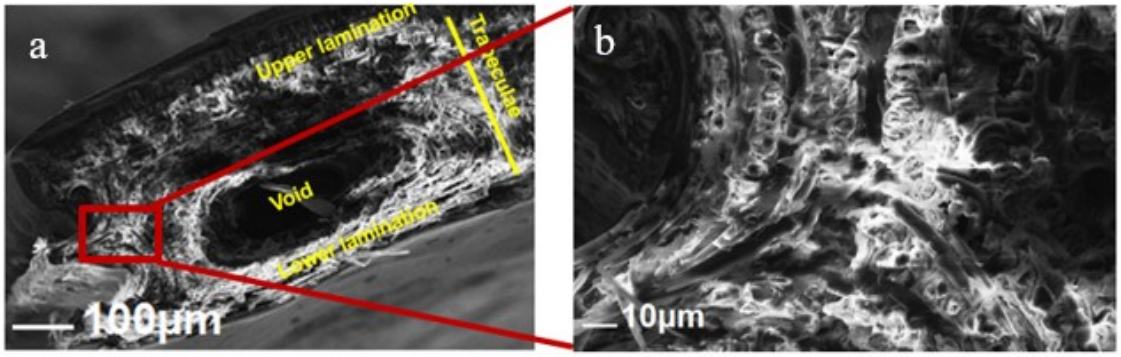


Figure 4.5 SEM images of the fracture elytron's cross section: (a) a brick-like structure seen in other beetle's elytra is observed and labeled accordingly, and (b) a higher magnification SEM showing the arrangement of the chitin-protein planes around the brick structure.

Figure 4.5 shows a lamellar structure that comprises the elytron. Each "brick" of the lamellar structure contains a void surrounded by curved chitin-protein fiber planes. Figure 4.6 shows a model of voids throughout the exoskeleton. The voids geometry was

created with the microCT scans and ScanIP™ (Simpleware, Exeter, UK). The voids have a distinct pattern that runs through the entire exoskeleton. The lamellar structure has been observed in elytra of Cotinis mutabilis by Yang and of A. dichotoma by He and Chen (Yang 2017; He 2015). In addition to the elytron, He found the lamellar structure in the fore-wing of A. dichotoma (He 2015). These studies labeled the upper border of the "brick" as upper lamination, lower border as the lower lamination, and the vertical chitin-fiber planes between two bricks as the trabeculae; Figure 4.6 is labeled in accordance. In previous studies, the exoskeleton and fore-wing consist primarily of the voids while the ironclad beetle does not. Possible differences between the lamellar structures of the ironclad beetle to other beetles could be caused by the fusion of the exoskeleton with the wings based on their function. *A. dichotoma*'s elytron is structured to enhanced flight, while the ironclad beetle's elytron does not need to (He 2015). The width of the trabeculae is similar to the length of the larger pattern season on the surface of the elytron. One example of bio-inspired design studies has replicated the lamellar microstructure lightweight, high-performance structures (Munch 2008). Impacts into the lamellar structure would cause a sliding movement increasing the friction of the deformation and increasing the crack toughness of the structure (Munch 2008).

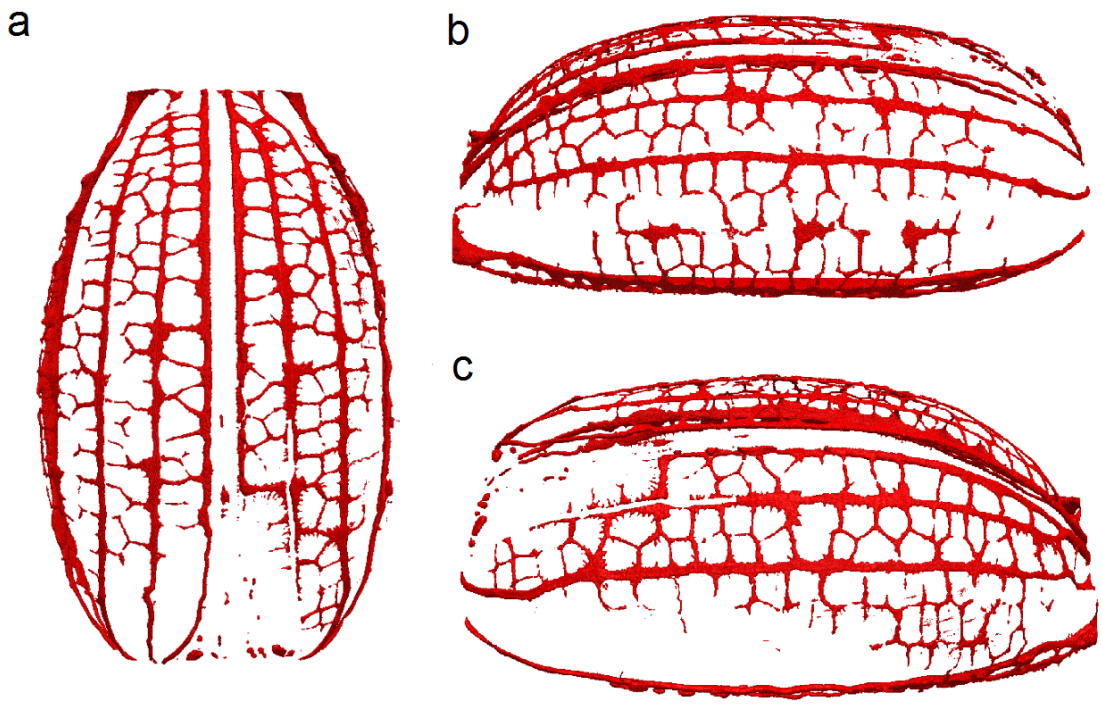


Figure 4.6 Simpleware 3D model of the "tunnel-like" voids in the ironclad beetle's exoskeleton created using the microCT scans from (a) top, (b) medial, and (c) lateral views. These voids run along the elytra's anteroposterior axis along with smaller interconnecting "tunnel-like" voids in the lateral plane. This model was created by modeling the negative volume in the elytron.

.

## 4.4 Chemical Composition

Table 4.1 reveals the chemical composition on the top and bottom surface of pronotum and elytron. Various elements were found in each sample including various metals. Surface analysis showed the existence of minerals in all four surfaces. The carbon, nitrogen, and oxygen found in the elytron bottom. Nitrogen found in the structure

can be attributed by the α-chitin found in the exoskeleton, $C_8H_{13}O_5N$ (Chen 2008). Unlike the pronotum bottom, the elytron bottom could consist of chitin because the wing structure fusion.

Table 4.1 Chemical composition of the pronotum and elytron top and bottom surfaces

| | % of Total Composition | | | |
|---|---|---|---|---|
| | Pronotum | | Elytron | |
| | Top | Bottom | Top | Bottom |
| C | 81.35 | 82.81 | 79.95 | 72.71 |
| O | 15.84 | 14.26 | 17.46 | 12.62 |
| N | - | - | - | 13.59 |
| K | - | 0.07 | 0.05 | - |
| Fe | 0.25 | - | 0.03 | 0.04 |
| Zn | 2.32 | 2.48 | 2.37 | 1.02 |
| Cl | 0.09 | 0.20 | 0.13 | - |
| Mn | 0.11 | 0.09 | - | - |
| Ca | 0.04 | 0.09 | - | 0.03 |
| Metals | 2.70 | 2.66 | 2.67 | 1.09 |

Chemical composition of the pronotum and elytron top and bottom surfaces.

Chemical composition of the cross section of pronotum and elytron were also conducted for each layer. The cross section also showed the existence of nitrogen in exocuticle and endocuticle layers as to be expected because those layers are made of

chitin. In addition to zinc, iron, calcium, and manganese, the minerals magnesium and silicon were found in the cross section. Reichle (1969) noted that calcium, potassium, and sodium have been found in forest floor insects from debris in the environment and their diets. The ironclad beetle is known to be a forest insect and could contain these same elements because of its environment or diet.

In addition, we found an existence of elements that could be associated to minerals such as calcium carbonate, iron oxide, zinc oxide, and manganese oxide in the exoskeleton. The existence of these minerals could add to the mechanical strength of the exoskeleton. Calcium carbonate was observed in the lobster exoskeleton, and iron oxide, zinc oxide, and manganese have seen in insect exoskeletons (Vincent 2004). Discussion of the effect of mineralization on the structure is found in section 4.7.

## 4.5 Nano-indentation

Table 4.2 Mechanical properties of the pronotum and elytron top and bottom surfaces

| | | Loading Rates (μN/s) | | | | | |
|---|---|---|---|---|---|---|---|
| | | 1 | | 10 | | 100 | |
| Location | | $E_r$ (GPa) | H (MPa) | $E_r$ (GPa) | H (MPa) | $E_r$ (GPa) | H (MPa) |
| Pronotum | Top | 6.49±0.12 | 639.46±1.65 | 8.38±0.37 | 475.23±36.62 | 8.85±0.20 | 490.48±3.63 |
| | Bottom | 1.44±0.02 | 125.54±1.82 | 2.00±0.07 | 215.45±15.72 | 2.60±0.04 | 260.85±7.64 |
| Elytron | Top | 3.32±0.09 | 422.35±25.42 | 5.21±0.09 | 364.29±10.89 | 6.51±0.011 | 441.08±15.13 |
| | Bottom | 2.74±0.1 | 281.93±7.88 | 3.88±0.07 | 261.57±4.95 | 4.00±0.04 | 250.62±2.17 |

Four surface locations (pronotum top and bottom and elytron top and bottom) were indented at three different loading rates (1, 10, and 100 μN/s) at a peak load of 500 μN and a holding time of 20s. Each test had an unloading rate equal to the loading rate. Each loading rate produced a different reduced elastic modulus ($E_r$) and hardness value (H) as shown in Table 4.2. The pronotum top surface had higher reduced elastic modulus and hardness values, then the elytron top surface, elytron bottom, and the pronotum bottom. The differences between the reduced elastic modulus and hardness of each surface is discussed further in section 4.7. As the loading rate increased, reduced elastic modulus increased. This is consistent with other studies analyzing the loading-rate dependency of viscoelastic materials (Fan and Rho 2003). Nano-indentation testing at lower loading rates allow the material more time to respond to the applied load.

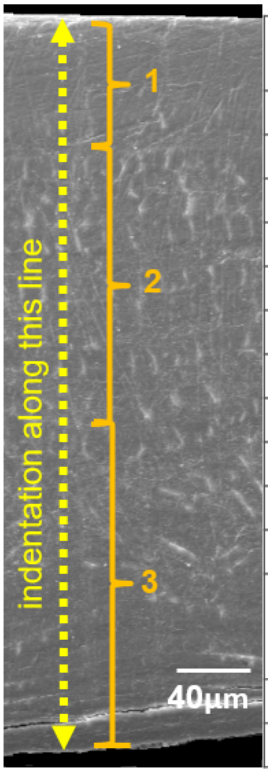


| Composition (%) | 1: Epicuticle | 2: Exocuticle | 2: Endocuticle |
|---|---|---|---|
| C | 77.28 | 70.83 | 65.24 |
| O | 18.96 | 12.23 | 19.96 |
| N | - | 13.52 | 13.33 |
| K | 0.15 | 0.12 | 0.20 |
| Fe | 0.42 | 0.41 | 0.41 |
| Zn | 2.44 | 2.51 | - |
| Cl | - | 0.22 | 0.36 |
| Mn | 0.09 | 0.59 | 0.14 |
| Ca | 0.11 | - | 0.14 |
| Mg | - | - | 0.02 |
| Na | - | - | 0.20 |
| **Mechanical Properties (GPa)** | **1: Epicuticle** | **2: Exocuticle** | **2: Endocuticle** |
| $E_R$ | 3.02 | 2.66 | 4.69 |
| H | 0.16 | 0.17 | 0.35 |

Figure 4.7 Reduced elastic modulus and hardness values obtained from nanoindentation along the cross section of the pronotum.

Due to the layered structure of the pronotum and elytron, the cross section of both were tested under nano-indentation with the loading and unloading rate of 10 µN/s at a peak load of 500 µN/s and a holding time of 20s. The location of indentation for the pronotum and elytron and the corresponding mechanical properties and chemical composition for each layer are shown in Figure 4.7 and Figure 4.8 respectively. For the pronotum, the endocuticle had the highest reduced elastic modulus and hardness values followed by the pore canals then the exocuticle. In the elytron, the areas with the highest

mechanical properties were the exocuticle and endocuticle then the pore canals and brick structure.

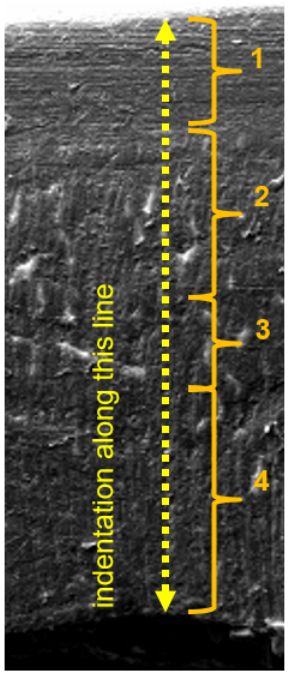


| Composition (%) | 1: Epicuticle | 2: Exocuticle | 3: Endocuticle | 4: Brick |
|---|---|---|---|---|
| C | 87.17 | 70.11 | 72.32 | 72.81 |
| O | 7.22 | 11.07 | 12.86 | 10.22 |
| N | - | 14.04 | 11.65 | 13.01 |
| K | - | 0.15 | 0.09 | 0.07 |
| Fe | 0.58 | 0.04 | - | 0.56 |
| Zn | 4.39 | 2.67 | 2.68 | 2.76 |
| Cl | 0.17 | 0.17 | 0.20 | 0.21 |
| Mn | 0.27 | 0.16 | 0.04 | 0.19 |
| Ca | 0.20 | - | 0.06 | - |
| Mg | - | - | 0.09 | - |
| Si | - | - | - | 0.17 |
| **Mechanical Properties (GPa)** | **1: Epicuticle** | **2: Exocuticle** | **3: Endocuticle** | **4: Brick** |
| $E_R$ | 10.02 | 22.82 | 13.21 | 7.22 |
| H | 0.28 | 0.66 | 0.49 | 0.27 |

Figure 4.8 Reduced elastic modulus and hardness values obtained from nano-indentation along the cross section of the elytron.

## 4.6 Structure-Property Relationship

The ironclad beetle's exoskeleton has several characteristics that could attribute to its strength. Length characterization revealed the thickness of the exoskeleton. Both the thickness of the pronotum and elytron were thicker than any other exoskeleton known in

the published literature. Increased thickness of the exoskeleton could correlate to increased density of chitin-fiber planes providing increased toughness against fractures.

Alternatively, the thickness could be attributed to a thicker epicuticle layer. SEM revealed a layer between the surface of the elytron and pronotum and the exocuticle referred to by the epicuticle. SEM revealed the bulk of the epicuticle in the ironclad beetle consisted of wax pore canals, which transfer wax materials to the surface (Wigglesworth 1985). The increased thickness of the epicuticle, compared to other exoskeletons, could provide more space between possible water penetration and the chitin. Dehydration of the chitin fibers is important to maintain its strength. Hydrogen bonds are important to maintain the α-chitin structure and the Bouligand structure.

An arrangement of anti-parallel chitin (α-chitin) and parallel-chitin (β-chitin) is shown in Figure 4.9. α-chitin that is found in insect exoskeleton is hard and rigid, while β-chitin found in jellyfish is soft and flexible (Campana-Filho 2007). The main difference between the two forms, and why one is hard or one is soft, is the number of hydrogen bonds. The addition of water to chitin would destabilize the hydrogen bond and reduced the mechanical properties (Hillerton 1979). Due to the increased thickness of the epicuticle and the increased amount of wax, it is more difficult for water to penetrate, reach the chitin heavy layers (the exocuticle and endocuticle), and disrupt the hydrogen bonding.

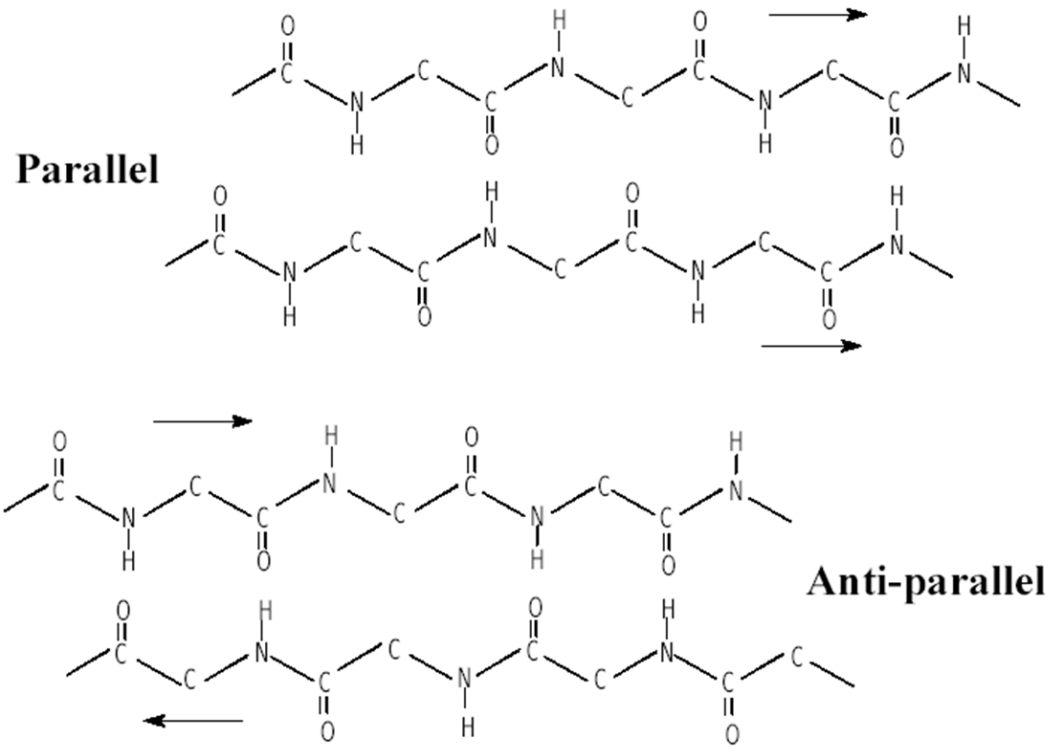


Figure 4.9 Hydrogen boding between α-chitin and β-chitin. A-chitin is arranged in an anti-parallel order, while β-chitin is arranged in a parallel fashion.

In addition, the increased number of pore canals could also strengthen the structure. As mentioned previously, Sachs simulated loading and found deformation in the planes were minimized due to the collapse of the pore canals (Sachs 2008). The number of pore canals could increase the resistance from tensile loading thus enhancing the structure (Cribb 2010). The ironclad beetle's epicuticle contained an increased

number of pore canals that were also longer, and the exoskeletal structure could be greatly enhanced and have great resistance against tensile loading.

The effects of the mineralization on the mechanical properties of the exoskeletons and many biological structures have been extensively studied (Anderson 2010). For insects, specifically the existence of zinc and manganese have been shown to harden exoskeletons. Minerals typically indicate a higher fracture toughness cuticle compared to non-mineralized cuticles (Quicke 1998; Hillerton 1984; Al-Sawalmih 2008; Anderson 2010). Zinc has been shown to increase the mechanical properties of the structure by 20%, while manganese does not have the same significant effect (Hillerton 1984; Cribb 2010). This evidence makes the authors believe each metal effects the structure at different degrees making it difficult to quantify which mineral attributes the most to the ironclad beetle's exoskeleton. Unlike zinc and manganese, the effect of iron has not been extensively studied. Iron oxide has been found in few exoskeletons and is believed to increase the hardness of a biological tissues (Vincent 2004). Because the ironclad beetle is believed to be uniquely tough, the incorporation of iron could be a key component of why the structure is tough.

An example that could provide evidence of this concept is the difference in mechanical properties of the top and bottom surface of the pronotum. Top surface is significantly harder than the bottom surface. In terms of metal composition, the main difference to explain why the top surface is harder than the bottom surface is the existence of iron on the top surface.

In general, the appearance of minerals has been the link to harder and stiffer materials. In addition, structural investigations of chitin support the belief of more than

one binding site for metal on chitin (Gamblin 1998). If this is true, the variation of metals (Zn, Mn, Fe, Ca, Mg) could benefit the production of a tougher structure if chitin is involved.

## 4.7 Hierarchical Structure

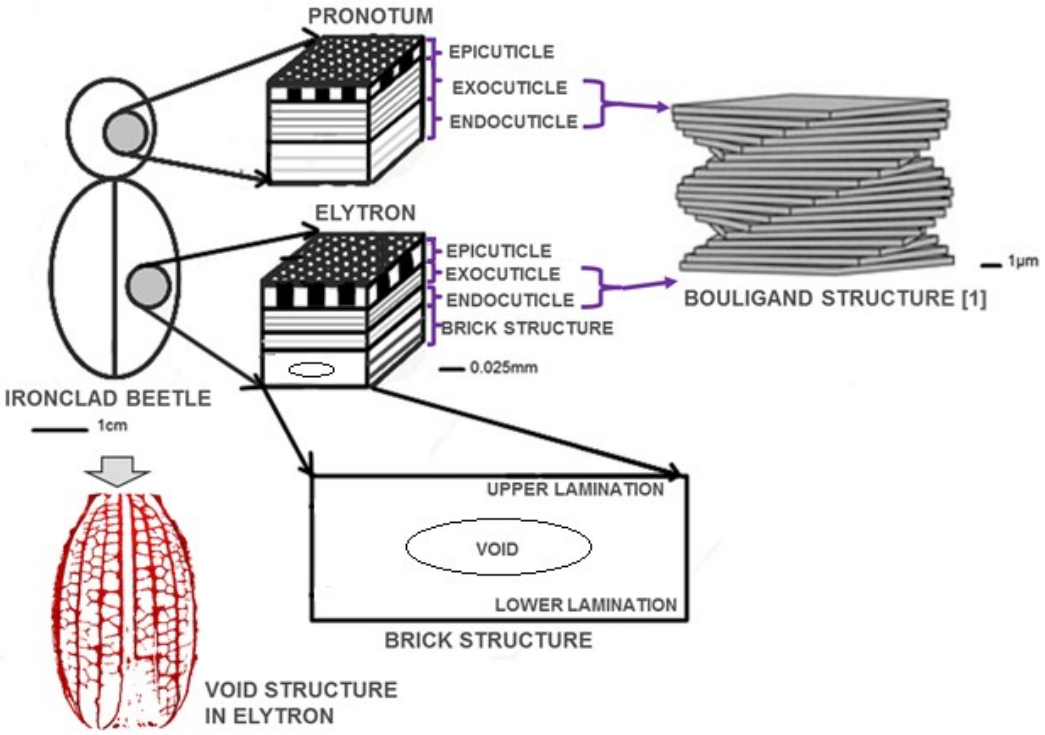


Figure 4.10 Proposed hierarchical structure of the ironclad beetle.

To more fully understand the structure-property relationships within the exoskeleton, the structure of the beetle was evaluated utilizing the aforementioned methods. Biological materials are unique in comparison to other materials because they have a hierarchical structure (Xia 2008). The results of the study suggest the ironclad beetle has a similar hierarchical structure to other arthropods. The proposed hierarchical structure of the ironclad beetle is shown in Figure 4.9. Microstructure observation of the cross section with the fracture and cut surface show the existence of the Bouligand structure in the form of chitin-protein planes. At its lowest structure, N-acetyl-D-glucosamine is synthesized into chitin molecules. Chitin has a similar hierarchy to collagen; that is chitin builds from molecules to microfibers to fibers. The chitin nanofibers are surrounded by proteins and place into a chitin-protein matrix forming larger fibers. These fibers are placed into a plane that are then stacked into a Bouligand structure. This Bouligand structure composes the endocuticle and exocuticle layer that attributed to most of the exoskeleton's structure and strength. In regard to the pronotum and elytra, the structure begins to change. The pronotum contains the layered structured seen in the lobster and crab exoskeletons with no voids, while the elytron is comprised of the laminar brick structure where the chitin fibers wrap around a "tunnel-like" voids and each "brick" is divided by trabecula. The voids run throughout the elytron as shown by the model created by the microCT in Figure 4.6. Further examination will need to be conducted to analyze the location of metals in the structure of the ironclad beetle.

# CHAPTER V

# CONCLUSIONS

The goal of the present study aim is to determine the structure-property relationships of the ironclad beetle's exoskeleton. We completed three steps to accomplish this goal: analyze the microstructure of the exoskeleton through optical observation and chemical analysis, perform nano-indentation on the exoskeleton to determine the mechanical properties, and correlate the microstructure to the mechanical properties. Using this information, structure-property relationships within the exoskeleton were determined.

Structure and chemical observations allowed determination of the key components of the structure and their composition. This was conducted using microCT, SEM, EDS, and AFM. Images collected from microCT and SEM underwent analysis using image to determine lengths of various aspects of the structure. MicroCT scans were also analyzed in Bruker Skyscan Control and ScanIP (Simpleware, Exeter, UK).

Results show the ironclad beetle's exoskeleton has a similar hierarchy to previously studied arthropods such as crustaceans and other beetle exoskeletons. The exoskeleton is a layered composite consisting primarily of chitin-protein fiber planes in a

Bouligand structure. The layers in the exoskeleton that were observed were the epicuticle, exocuticle, and endocuticle. The structure of the pronotum is a uniform composite with stratified layers similar to the structure of crustacean exoskeletons. The structure of the elytron is in a lamellar "brick" structure found in elytron of previous studied beetles but is different in that the "tunnel-like" voids occur less frequently. This lamellar microstructure has been seen in characteristic design in tough materials by increasing crack resistance. The tunnel-like voids provide a lighter exoskeleton in weight but does not significantly weaken the system because it is reinforced by continuous chitin-fibers around the void.

In both the pronotum and elytron, the epicuticle was thicker than previously reported exoskeletons. SEM showed the bulk of the epicuticle contained wax pore canals filled with wax. The purpose of the wax pore canals is to transfer wax materials to the surface of the exoskeleton. It was proposed the thickness of the epicuticle and increased amount of wax purposely prevented water penetration into the exoskeleton that would disrupt the α-chitin structure.

EDS revealed the existence of minerals in the form of iron oxide, manganese oxide, zinc oxide, calcium carbonate and others in the exoskeleton. These minerals were not observed through SEM images but have been seen in observations of exoskeletons of other arthropod species. Iron oxide, manganese oxide, and zinc oxide have been shown to increase the hardness of the insect cuticle to varying degrees, while calcium carbonate has been seen to increase the hardness of crustacean cuticles. While other cuticles have contained these minerals, this exoskeleton is the only exoskeleton to contain this quantity and variety of minerals to the author's knowledge. In addition, the ironclad beetle's

exoskeleton in comparison to other beetles' exoskeletons had a thicker exoskeleton. The ironclad beetle is the only beetle to the author's knowledge to be studied where the wings are fused into the elytra. It is proposed the existence and variety of minerals also contributed to the exoskeleton's hardness. This is supported by the results of the nano-indentation testing.

The characteristics of the exoskeleton observed to provide strength to the structure are the chitin-protein planes, the strengthening of the structure by the addition of minerals, and the lamellar microstructure found in the elytron exoskeleton. The suggested uniqueness of the ironclad beetle in comparison to other exoskeletons is the thickness of its exoskeleton that adds strength through bulk and the existence of variety and quantity of different minerals.

# CHAPTER VI

# FUTURE WORKS

As previously stated, this study acts as the first phase of a bio-inspired design study on the ironclad beetle exoskeleton. This study revealed many key components of the exoskeleton and many structure-property relationships that could be incorporated into a future bio-inspired 3D prototype. However, these key components and structure-property relationships must be investigated further to understand its full impact on the overall structure of the exoskeleton.

A detailed comparison of various beetles would allow a better determination of the unique properties of the ironclad beetle. Literature featuring beetles with a fused exoskeleton was lacking, thus it is unknown if certain key components are unique to the ironclad beetle or fused beetle, such as the existence of chitin on the bottom surface layer of the elytron. In addition, knowing if the percentage of volume taken up by the voids different from beetle to beetle and how that percentage varies compared to the fracture toughness could provide useful information.

A key component of the exoskeleton was the Bouligand structure and chitin-fiber planes. The exoskeleton of the ironclad beetle was thicker than previously researched exoskeletons. The increased thickness could be contributed to the increased length of the wax pore canals and the increased number of chitin-fiber planes. The increased number of chitin-fiber planes is proposed to strongly effect the fracture and bending toughness of the exoskeleton. Further investigation into the impact resistance of plywood structures and the effects of the 180° twist would provide additional knowledge of all Bouligand structures. This investigation could lead to the production of an optimized plywood material.

The role of the minerals in the ironclad beetle is not completely understood. The minerals increase the mechanical properties, but the underlying mechanism is unclear. The method to which the minerals stiffens or hardness the chitin could allow the development of stiffer fibers in the future. Outside of the exoskeleton, the structure of the beetle could be useful to analyzed. Both performance of the exoskeleton and the beetle as a whole should be determined under higher-scale testing such as bending, shear, or high-rate testing. This could be done with experiments or through finite element analysis. Finite element analysis could use the microCT scans and import a model using ScanIP.

The eventual goal of this bioinspired study is to create a 3D prototype for an impact resistant technology. As of now, the ironclad beetle could be used to produce stiffer fibers or a lightweight structure such as a bulletproof vest that needs to be tough against fracture, bending, or impacts.

REFERENCES


Zolotovsky, K. (2012). *BioConstructs: methods for bio-inspired and bio-fabricated design* (Doctoral dissertation, Massachusetts Institute of Technology).

Liu, K., & Jiang, L. (2011). Bio-inspired design of multiscale structures for function integration. *Nano Today*, 6(2), 155-175.

Naleway, S. E., Porter, M. M., McKittrick, J., & Meyers, M. A. (2015). Structural design elements in biological materials: application to bioinspiration. *Advanced Materials*, 27(37), 5455-5476.

Meyers, M. A., Chen, P. Y., Lin, A. Y. M., & Seki, Y. (2008). Biological materials: structure and mechanical properties. *Progress in Materials Science*, 53(1), 1-206.

Lakes, R. (1993). Materials with structural hierarchy. Nature, 361(6412), 511-515.

Chen, B., Peng, X., Wang, W., Zhang, J., & Zhang, R. (2002). Research on the microstructure of insect cuticle and the strength of a biomimetic preformed hole composite. *Micron*, 33(6), 571-574.

Jensen, M., & Weis-Fogh, T. (1962). Biology and physics of locust flight. V. Strength and elasticity of locust cuticle. *Philosophical Transactions of the Royal Society of London B: Biological Sciences*, 245(721), 137-169..

Locke, M. (1964). The structure and formation of the integument in insects. In *The physiology of Insecta* (Vol. 3, pp. 379-470). Academic Press New York.

De Renobales, M., Nelson, D. R., & Blomquist, G. J. (1991). Cuticular lipids. *The Physiology of the Insect Epidermis*, 240-251.

Noble-Nesbitt, J. (1991). Cuticular permeability and its control. *Physiology of the insect epidermis*, 252-283.

Chen, P. Y., Lin, A. Y. M., Lin, Y. S., Seki, Y., Stokes, A. G., Peyras, J., & McKittrick, J. (2008). Structure and mechanical properties of selected biological materials. *Journal of the Mechanical Behavior of Biomedical Materials*, 1(3), 208-226.

Minke, R. A. M., & Blackwell, J. (1978). The structure of α-chitin. *Journal of molecular biology*, 120(2), 167-181.

Blackwell, J., & Weih, M. A. (1980). Structure of chitin-protein complexes: Ovipositor of the ichneumon fly Megarhyssa. *Journal of molecular biology*, 137(1), 49-60.

Raabe, D., Sachs, C., & Romano, P. (2005). The crustacean exoskeleton as an example of a structurally and mechanically graded biological nanocomposite material. *Acta Materialia*, 53(15), 4281-4292.

Vincent, J. F., & Wegst, U. G. (2004). Design and mechanical properties of insect cuticle. *Arthropod structure & development*, 33(3), 187-199.

Andersen, S. O., Hojrup, P., & Roepstorff, P. (1995). Insect cuticular proteins. *Insect biochemistry and molecular biology*, 25(2), 153-176.

Andersen, S. O., & Weis-Fogh, T. (1964). Resilin. A rubberlike protein in arthropod cuticle. *Advances in insect physiology*, 2, 1-65.

HILLERTON, J. E., & VINCENT, J. F. (1982). The specific location of zinc in insect mandibles. *Journal of Experimental Biology*, 101(1), 333-336.

Hepburn, H. R., & Chandler, H. D. (1980). Materials testing of arthropod cuticle preparations. In *Cuticle Techniques in Arthropods* (pp. 1-44). Springer New York.

Wigglesworth, V. B. (1950). The principles of insect physiology. *The Principles of Insect Physiology*., (Edn 4).

Anderson, M. B., Preslan, J. E., Jolibois, L., Bollinger, J. E., & George, W. J. (1997). Bioaccumulation of lead nitrate in red swamp crayfish (Procambarus clarkii). *Journal of hazardous materials*, 54(1-2), 15-29.

Wigglesworth, V. B. (1972). Digestion and nutrition. In *The principles of insect physiology* (pp. 476-552). Springer Netherlands.

Gunderson, S., & Schiavone, R. (1989). The insect exoskeleton: a natural structural composite. *Journal of the Minerals, Metals and Materials Society*, 41(11), 60-63.

Neville, A. C. (1984). Cuticle: organization. In *Biology of the Integument* (pp. 611-625). Springer Berlin Heidelberg.

Andersen, S. O. (1979). Biochemistry of insect cuticle. *Annual review of entomology*, 24(1), 29-59.

Locke, M. (1961). Pore canals and related structures in insect cuticle. *The Journal of Cell Biology*, 10(4), 589-618.

Sachs, C., Fabritius, H., & Raabe, D. (2006). Experimental investigation of the elastic–plastic deformation of mineralized lobster cuticle by digital image correlation. *Journal of structural biology*, 155(3), 409-425.

Sachs, C., Fabritius, H., & Raabe, D. (2008). Influence of microstructure on deformation anisotropy of mineralized cuticle from the lobster Homarus americanus. *Journal of Structural Biology*, 161(2), 120-132.

Tong, J., Sun, J. Y., Chen, D. H., & Zhang, S. J. (2004). Factors impacting nanoindentation testing results of the cuticle of dung beetle Copris ochus Motschulsky. *Journal of Bionics Engineering*, 1(4), 221-230.

Vincent, J. F. (2002). Arthropod cuticle: a natural composite shell system. *Composites Part A: Applied Science and Manufacturing*, 33(10), 1311-1315.

Kumar, M. N. R. (2000). A review of chitin and chitosan applications. *Reactive and functional polymers*, 46(1), 1-27.

Fox, J. D., Capadona, J. R., Marasco, P. D., & Rowan, S. J. (2013). Bioinspired water-enhanced mechanical gradient nanocomposite films that mimic the architecture and properties of the squid beak. *Journal of the American Chemical Society*, 135(13), 5167-5174.

Hamed, I., Özogul, F., & Regenstein, J. M. (2016). Industrial applications of crustacean by-products (chitin, chitosan, and chitooligosaccharides): A review. *Trends in Food Science & Technology*, 48, 40-50.

Wu, J., & Meredith, J. C. (2014). Assembly of chitin nanofibers into porous biomimetic structures via freeze drying. *ACS Macro Letters*, 3(2), 185-190.

QUICKE, D. L., Wyeth, P., Fawke, J. D., Basibuyuk, H. H., & Vincent, J. F. (1998). Manganese and zinc in the ovipositors and mandibles of hymenopterous insects. *Zoological Journal of the Linnean Society*, 124(4), 387-396.

Hillerton, J. E., Robertson, B., & Vincent, J. F. (1984). The presence of zinc or manganese as the predominant metal in the mandibles of adult, stored-product beetles. *Journal of Stored Products Research*, 20(3), 133-137.

Al-Sawalmih, A., Li, C., Siegel, S., Fabritius, H., Yi, S., Raabe, D., & Paris, O. (2008). Microtexture and chitin/calcite orientation relationship in the mineralized exoskeleton of the American lobster. *Advanced Functional Mat*erials, 18(20), 3307-3314.

Lian, J., & Wang, J. (2014). Microstructure and mechanical anisotropy of crab cancer magister exoskeletons. *Experimental Mechanics*, 54(2), 229-239.

Nikolov, S., Petrov, M., Lymperakis, L., Friák, M., Sachs, C., Fabritius, H. O., ... & Neugebauer, J. (2010). Revealing the design principles of high-performance

biological composites using ab initio and multiscale simulations: the example of lobster cuticle. *Advanced Materials*, 22(4), 519-526.

Dittman, E. K., & Buchwalter, D. B. (2010). Manganese bioconcentration in aquatic insects: Mn oxide coatings, molting loss, and Mn (II) thiol scavenging. *Environmental science & technology*, 44(23), 9182-9188.

Mann, S. (Ed.). (1995). Biomimetic materials chemistry. John Wiley & Sons.

Fabritius, H. O., Sachs, C., Triguero, P. R., & Raabe, D. (2009). Influence of Structural Principles on the Mechanics of a Biological Fiber-Based Composite Material with Hierarchical Organization: The Exoskeleton of the Lobster Homarus americanus. *Advanced materials*, 21(4), 391-400.

Lian, J., & Wang, J. (2014). Microstructure and mechanical anisotropy of crab cancer magister exoskeletons. *Experimental Mechanics*, 54(2), 229-239.

Chen, P. Y., Lin, A. Y. M., McKittrick, J., & Meyers, M. A. (2008). Structure and mechanical properties of crab exoskeletons. *Acta biomaterialia*, 4(3), 587-596.

Fabritius, H., Sachs, C., Raabe, D., Nikolov, S., Friák, M., & Neugebauer, J. (2011). Chitin in the exoskeletons of arthropoda: From ancient design to novel materials science. In *Chitin* (pp. 35-60). Springer Netherlands.

Boßelmann, F., Romano, P., Fabritius, H., Raabe, D., & Epple, M. (2007). The composition of the exoskeleton of two crustacea: The American lobster Homarus americanus and the edible crab Cancer pagurus. *Thermochimica Acta*, 463(1), 65-68.

Raabe, D., Romano, P., Sachs, C., Fabritius, H., Al-Sawalmih, A., Yi, S. B., ... & Hartwig, H. G. (2006). Microstructure and crystallographic texture of the chitin–protein network in the biological composite material of the exoskeleton of the lobster Homarus americanus. *Materials science and engineering*: A, 421(1), 143-153.

Romano, P., Fabritius, H., & Raabe, D. (2007). The exoskeleton of the lobster Homarus americanus as an example of a smart anisotropic biological material. *Acta Biomaterialia*, 3(3), 301-309.

Nikolov, S., Fabritius, H., Petrov, M., Friák, M., Lymperakis, L., Sachs, C., ... & Neugebauer, J. (2011). Robustness and optimal use of design principles of arthropod exoskeletons studied by ab initio-based multiscale simulations. *Journal of the mechanical behavior of biomedical materials*, 4(2), 129-145.

Hepburn, H. R., & Ball, A. (1973). On the structure and mechanical properties of beetle shells. *Journal of Materials Science*, 8(5), 618-623.

Sun, J., & Bhushan, B. (2012). Structure and mechanical properties of beetle wings: a review. *Rsc Advances*, *2*(33), 12606-12623.

Chen, J., Ni, Q. Q., Xu, Y., & Iwamoto, M. (2007). Lightweight composite structures in the forewings of beetles. *Composite Structures*, *79*(3), 331-337.

Cheng, H., Chen, M., & Sun, J. (2002). Histological structures of the dung beetle, Copris ochus Motschulsky integument. *Kun chong xue bao. Acta entomologica Sinica*, *46*(4), 429-435.

Chen, J., Dai, G., Xu, Y., & Iwamoto, M. (2007). Optimal composite structures in the forewings of beetles. *Composite Structures*, *81*(3), 432-437.

Chen, J., Xie, J., Wu, Z., Elbashiry, E. M. A., & Lu, Y. (2015). Review of beetle forewing structures and their biomimetic applications in China:(I) On the structural colors and the vertical and horizontal cross-sectional structures. *Materials Science and Engineering: C*, *55*, 605-619.

Gunderson, S. L., & Lute, J. A. (1993). The use of preformed holes for increased strength and damage tolerance of advanced composites. *Journal of reinforced plastics and composites*, *12*(5), 559-569.

SUN, J. Y., Jin, T. O. N. G., CHEN, D. H., LIN, J. B., LIU, X. P., & WANG, Y. M. (2010). Micro-tensile testing of the lightweight laminated structures of beetle elytra cuticle. *Advances in Natural Science*, *3*(2), 225-234.

Foley, I. A., & Ivie, M. A. (2008). A revision of the genus Phellopsis LeConte (Coleoptera: Zopheridae). *Zootaxa*, *1689*, 1-28.

Burke, H. R. (1976). beetle Zopherus nodulosus haldemani; symbol of the Southwestern Entomological Society. *Southwestern entomologist*.

Bartlett, T., & VanDyk, J. (n.d.). Texas Ironclad Beetle - Zopherus nodulosus - BugGuide.Net. Retrieved August 29, 2014, from http://bugguide.net/node/view/679394

Quinn, M. (n.d.). Texas Beetle Information. Retrieved October 09, 2017, from http://texasento.net/Ironclad.html

Lord, N.P, Nearns, E.H., and K.B. Miller. 2011-2013. Ironclad ID: Tool for Diagnosing Ironclad and Cylindrical Bark Beetles (Coleoptera: Zopheridae) of North America

north of Mexico. The University of New Mexico and Center for Plant Health Science and Technology, USDA, APHIS, PPQ.

Leary, SL., Underwood, W., Anthony, R., Gwaltney-Brant, S., Poison, A. S. P. C. A., & Meyer, R. (2013). AVMA guidelines for the euthanasia of animals: 2013 edition. Schaumburg, IL: American Veterinary Medical Association.

Oliver, W. C., & Pharr, G. M. (1992). An improved technique for determining hardness and elastic modulus using load and displacement sensing indentation experiments. *Journal of materials research*, *7*(6), 1564-1583.

Fischer-Cripps, A. C. (2000). *Introduction to contact mechanics* (p. 87). New York: Springer.

Sun, J., Ling, M., Wang, Y., Chen, D., Zhang, S., Tong, J., & Wang, S. (2014). Quasi-static and dynamic nanoindentation of some selected biomaterials. *Journal of Bionic Engineering*, *11*(1), 144-150.

Sun, J. Y., & Tong, J. (2007). Fracture toughness properties of three different biomaterials measured by nanoindentation. *Journal of Bionic Engineering*, *4*(1), 11-17.

Sun, J. Y., Tong, J., & Ma, Y. H. (2008). Nanomechanical behaviours of cuticle of three kinds of beetle. *Journal of Bionic Engineering*, *5*, 152-157.

Lian, J., & Wang, J. (2011). Microstructure and mechanical properties of dungeness crab exoskeletons. *Mechanics of Biological Systems and Materials*, *2*, 93-99.

Foley, I. A. (2006). *A review of the ironclad beetles of the world:(Coleoptera Zopheridae: Phellopsini and Zopherini)* (Doctoral dissertation, Montana State University-Bozeman, College of Agriculture).

Tubercle. Merriam-Webster 2017.

Foley, I. A., & Ivie, M. A. (2008). A revision of the genus Phellopsis LeConte (Coleoptera: Zopheridae). *Zootaxa*, *1689*, 1-28.

Locke, M. (1960). The cuticle and wax secretion in Calpodes ethlius (Lepidoptera, Hesperidae). *Journal of Cell Science*, *3*(55), 333-338.

Wigglesworth, V. B. (1985). The transfer of lipid in insects from the epidermal cells to the cuticle. *Tissue and Cell*, *17*(2), 249-265.

Yang, R., Zaheri, A., Gao, W., Hayashi, C., & Espinosa, H. D. (2017). AFM Identification of Beetle Exocuticle: Bouligand Structure and Nanofiber Anisotropic Elastic Properties. *Advanced Functional Materials*, *27*(6).

Zimmermann, E. A., Gludovatz, B., Schaible, E., Dave, N. K., Yang, W., Meyers, M. A., & Ritchie, R. O. (2013). Mechanical adaptability of the Bouligand-type structure in natural dermal armour. *Nature communications*, *4*.

He, C., Zu, Q., Chen, J., & Noori, M. N. (2015). A review of the mechanical properties of beetle elytra and development of the biomimetic honeycomb plates. *Journal of Sandwich Structures & Materials*, *17*(4), 399-416.

Munch, E., Launey, M. E., Alsem, D. H., Saiz, E., Tomsia, A. P., & Ritchie, R. O. (2008). Tough, bio-inspired hybrid materials. *Science*, *322*(5907), 1516-1520.

Reichle, D. E., Shanks, M. H., & Crossley Jr, D. A. (1969). Calcium, potassium, and sodium content of forest floor arthropods. *Annals of the Entomological Society of America*, *62*(1), 57-62.

Vincent, J. F., & Wegst, U. G. (2004). Design and mechanical properties of insect cuticle. *Arthropod structure & development*, *33*(3), 187-199.

Fan, Z., & Rho, J. Y. (2003). Effects of viscoelasticity and time-dependent plasticity on nanoindentation measurements of human cortical bone. *Journal of Biomedical Materials Research Part A*, *67*(1), 208-214.

Campana-Filho, S. P., Britto, D. D., Curti, E., Abreu, F. R., Cardoso, M. B., Battisti, M. V., ... & Lavall, R. L. (2007). Extraction, structures and properties of alpha-AND beta-chitin. *Química Nova*, *30*(3), 644-650.

Hillerton, J. E., & Vincent, J. F. V. (1979). STABILIZATION OF INSECT CUTICLES. *Journal of Insect Physiology*, *25*(12), 957.

Andersen, S. O. (2010). Insect cuticular sclerotization: a review. *Insect biochemistry and molecular biology*, *40*(3), 166-178.

QUICKE, D. L., Wyeth, P., Fawke, J. D., Basibuyuk, H. H., & Vincent, J. F. (1998). Manganese and zinc in the ovipositors and mandibles of hymenopterous insects. *Zoological Journal of the Linnean Society*, *124*(4), 387-396.

Al-Sawalmih, A., Li, C., Siegel, S., Fabritius, H., Yi, S., Raabe, D., ... & Paris, O. (2008). Microtexture and chitin/calcite orientation relationship in the mineralized exoskeleton of the American lobster. *Advanced Functional Materials*, *18*(20), 3307-3314.

Gamblin, B. E., Stevens, J. G., & Wilson, K. L. (1998). Structural investigations of chitin and chitosan complexed with iron or tin. *Hyperfine interactions*, *112*(1-4), 117-122.

Xia, F., & Jiang, L. (2008). Bio-inspired, smart, multiscale interfacial materials. *Advanced materials*, *20*(15), 2842-2858.